Title

Magnetic resonance biomarkers in radiation oncology: The report of AAPM Task Group 294

Journal

Medical Physics, 48(7)

ISSN

0094-2405

Authors

McGee, Kiaran P
Hwang, Ken-Pin
Sullivan, Daniel C
et al.

Publication Date

2021-07-01

DOI

10.1002/mp.14884

Magnetic resonance biomarkers in radiation oncology: The report of AAPM Task Group 294

Kiaran P. McGee[a)]
Department of Radiology, Mayo Clinic, Rochester, Minnesota, USA

Ken-Pin Hwang
Department of Imaging Physics, Division of Diagnostic Imaging, MD Anderson Cancer Center, University of Texas, Houston, Texas, USA

Daniel C. Sullivan
Department of Radiology, Duke University, Durham, North Carolina, USA

John Kurhanewicz
Department of Radiology, University of California, San Francisco, California, USA

Yanle Hu
Department of Radiation Oncology, Mayo Clinic, Scottsdale, Arizona, USA

Jihong Wang
Department of Radiation Oncology, MD Anderson Cancer Center, University of Texas, Houston, Texas, USA

Wen Li
Department of Radiation Oncology, University of Arizona, Tucson, Arizona, USA

Josef Debbins
Department of Radiology, Barrow Neurologic Institute, Phoenix, Arizona, USA

Eric Paulson
Department of Radiation Oncology, Medical College of Wisconsin, Milwaukee, Wisconsin, USA

Jeffrey R. Olsen
Department of Radiation Oncology, University of Colorado Denver - Anschutz Medical Campus, Denver, Colorado, USA

Chia-ho Hua
Department of Radiation Oncology, St. Jude Children's Research Hospital, Memphis, Tennessee, USA

Lizette Warner
Philips Medical Systems, Eindhoven, Netherlands

Daniel Ma
Department of Radiation Oncology, Mayo Clinic, Rochester, Minnesota, USA

Eduardo Moros
Department of Radiation Oncology, Moffitt Cancer Center, Tampa, Florida, USA

Neelam Tyagi
Department of Medical Physics, Memorial Sloan Kettering Cancer Center, New York, New York, USA

Caroline Chung
Department of Radiation Oncology, MD Anderson Cancer Center, University of Texas, Houston, Texas, USA

(Received 19 November 2020; revised 24 March 2021; accepted for publication 28 March 2021; published 20 May 2021)

Purpose: A magnetic resonance (MR) biologic marker (biomarker) is a measurable quantitative characteristic that is an indicator of normal biological and pathogenetic processes or a response to therapeutic intervention derived from the MR imaging process. There is significant potential for MR biomarkers to facilitate personalized approaches to cancer care through more precise disease targeting by quantifying normal versus pathologic tissue function as well as toxicity to both radiation and chemotherapy. Both of which have the potential to increase the therapeutic ratio and provide earlier, more accurate monitoring of treatment response. The ongoing integration of MR into routine clinical radiation therapy (RT) planning and the development of MR guided radiation therapy systems is providing new opportunities for MR biomarkers to personalize and improve clinical outcomes. Their appropriate use, however, must be based on knowledge of the physical origin of the biomarker signal, the relationship to the underlying biological processes, and their strengths and limitations. The purpose of this report is to provide an educational resource describing MR biomarkers, the techniques

used to quantify them, their strengths and weakness within the context of their application to radiation oncology so as to ensure their appropriate use and application within this field. © *2021 American Association of Physicists in Medicine* [https://doi.org/10.1002/mp.14884]

Key words: biomarker, imaging, MR, QIBA, quantitative, radiation therapy

Abbreviations

AAPM American Association of Physicists in Medicine
ACR American College of Radiology
ACRIN American College of Radiology Imaging Network
ADC Apparent Diffusion Coefficient
ADNI Alzheimer's Disease Neuroimaging Initiative
APTw Amide Proton Transfer Weighted Imaging
ASL Arterial Spin Labeling
AUC Area Under the Curve
BOLD Blood Oxygen-Level Dependent
CaP Calcium Phosphate
CBF Cerebral Blood Flow
CEST Chemical Exchange Saturation Transfer
Cho Choline
CNI Choline-containing compound-N-acetylaspartate Index
CI Confidence Interval
CT Computed Tomography
Cr Creatine
CRT Conventional Radiation Therapy
CSF Cerebral Spinal Fluid
CTV Clinical Target Volume
D Dimensional
DCE Dynamic Contrast Enhanced
DFS Disease Free Survival
DIPG Diffuse Intrinsic Pontine Glioma
DSC Dynamic Susceptibility Contrast
DTI Diffusion Tensor Imaging
DWI Diffusion-Weighted Imaging
EBM Evidence-Based Medicine
ECM Extracellular Matrix
EES Extravascular, Extracellular Space
EPI Echo Planar Imaging
FA Fractional Anisotropy
FDA Food and Drug Administration (United States)
FLAIR Fluid-Attenuated Inversion Recovery
fMRI Functional Magnetic Resonance Imaging
GBCA Gadolinium-Based Contrast Agent
GBM Glioblastoma Multiforme
GTV Gross Tumor Volume
HCC Hepatocellular Carcinoma
HP Hyperpolarization
HU Hounsfield Units
$IAUGC_{BN}$
Blood-Normalized Area-Under-the-Gadolinium-Concentration Curve
IMRT Intensity-Modulated Radiotherapy
ISMRM International Society of Magnetic Resonance in Medicine
LC Model
Linear Combination Model
LDH Lactate Dehydrogenase
LDHA Lactate Dehydrogenase A
K^{trans} Vasculature-extravascular extracellular space Transfer constant
MCTs Monocarboxylate Transporters
mIns Myo-inositol
mpMRI Multi parametric Magnetic Resonance Imaging
MR Magnetic Resonance
MRE Magnetic Resonance Elastography
MRI Magnetic Resonance Imaging
MRS MR Spectroscopy
MRSI MR Spectroscopic Imaging
MT Magnetization Transfer
MTR_{asym}
Asymmetric Magnetization Transfer Ratio
NAA N-AcetylAspartate
NADH Nicotinamide Adenine Dinucleotide + Hydrogen
NAFLD Nonalcoholic Fatty Liver Disease
NASH Nonalcoholic Steatohepatitis
NIH National Institutes of Health
NIST US National Institute of Standards and Technology
NSCLC Non-small Cell Lung Cancer
OHSCC Oropharyngeal and Hypopharyngeal Squamous Cell Carcinoma
PDFF Proton Density Fat Fraction
PDF-MRI
Perfusion, Diffusion, and Flow Magnetic Resonance Imaging
PET Positron Emission Tomography
PFS Progression-Free Survival
PRESS Point Resolved Spectroscopy
PRF Proton Resonant Frequency
PSA Prostate-Specific Antigen
PSMA Prostate-Specific Membrane Antigen
PTV Planning Target Volume
QA Quality Assurance
QC Quality Control
QIB Quantitative Imaging Biomarker
QIBA Quantitative Imaging Biomarkers Alliance
rCBV relative Cerebral Blood Volume
RANO Response Assessment in Neuro-Oncology criteria
ROC Receiver Operating Characteristic
RF Radiofrequency
RO Radiation Oncology
rsMRI Resting State (Functional) Magnetic Resonance Imaging
RSNA Radiologic Society of North America
RT Radiation Therapy
SBRT Stereotactic Body Radiation Therapy
SE Spin Echo
SPIO Superparamagnetic Iron Oxide

SNR Signal to Noise Ratio
STARD Standards for Reporting of Diagnostic Accuracy
STEAM Stimulated Echo Acquisition Mode
T Tesla
tCho/Cr Total Choline to Creatine Ratio
TNM Tumor, Node, Metastases
TOLD Tissue Oxygen Level Dependent
TRUS Transrectal Ultrasound
USPIO Ultra-small Superparamagnetic Iron Oxide
wCMA Weighted Center of Mass
XRT X-ray Radiation Therapy

TABLE OF CONTENTS

1. INTRODUCTION

A magnetic resonance (MR) biologic marker (biomarker) is a measurable quantitative characteristic that is an indicator of normal biological and pathogenetic processes or a response to therapeutic intervention derived from the MR imaging process.[1] There is significant potential for MR biomarkers to facilitate personalized approaches to cancer care through more precise quantification of normal vs pathologic tissue function, response to therapy as well as toxicity to both radiation and chemotherapy. The ongoing integration of MR into routine clinical radiation therapy (RT) planning and the development of MR-guided radiation therapy systems are providing new opportunities for MR biomarkers to personalize and improve clinical outcomes. Their appropriate use, however, must be based on knowledge of the physical origin of the biomarker signal, the relationship to the underlying biological processes, and their strengths and limitations. Additionally, while significant literature exists providing quantitative values associated with a range of MR biomarkers, these values would not be considered compliant with the stringent requirements necessary to classify the parameter as a quantitative MR biomarker. This is particularly true within the context of using these values to drive radiation oncology (RO) treatment decisions, the most notable of which relate to adaptive treatment planning and delivery. The overall objective of this report is to provide physicists and clinicians with a basic understanding of MR biomarkers within the context of RO. Clarification is provided in terms of the definition of an imaging biomarker as well as the criteria by which a biomarker is considered quantitative. Their physical bases, strengths and limitations, values for normative and disease processes, as well as response to therapy when known are presented. Finally, standardized approaches to quality control and quality assurance programs are described.

This educational report serves several purposes: (i) To describe the framework used to define an imaging biomarker and establish clinical validation, utility, and quantification, (ii) to identify MR biomarkers known to provide information relevant to RO, (iii) to describe standardized processes necessary for the quantification and validation of MR biomarkers in RO, and (iv) to provide quantitative values of these biomarkers under both normative and pathologic conditions.

While not all potential MR biomarkers for RO are described here, those considered most common and promising are reported. For those measurements that remain undiscovered or unclassified, it is the intent of this report to describe the framework required to translate such measurements into imaging biomarkers for RO application.

TABLE I. Stages of biomarker development adapted from Sorensen.[5]

Term / Stage	Definition
Pre-biomarker	Proof of concept establishing technical performance
Biomarker	Safety and reproducibility established but utility not yet clear
Surrogate	Qualified for use in drug development
Licensed	Used in therapeutic decision making

TABLE II. Biomarker classification based on type. Note the bracketed values for biomarker Type (0, I, III) reflect the nomenclature used by Frank et al[4] and have been included for the purposes of cross referencing.

Biomarker classification	Description
Type 0 (0)	Marker of the natural history of a disease and correlates longitudinally with known clinical indices
Type 1 (I)	Marker that captures the effects of a therapeutic intervention in accordance with its mechanism of action.
Type 2 (II)(surrogate endpoint)	Marker that is intended to substitute for a clinical endpoint and expected to predict clinical benefit (or harm or lack of benefit or harm) on the basis of epidemiological, therapeutic, pathophysiological, or other scientific evidence.

2. DEFINITIONS

In 2001, in response to the rapid growth of new molecular based drug therapies and the need to provide more expeditious assessment of therapeutic efficacy, the National Institutes of Health described the concept of a biological marker (biomarker)[2] as being "A characteristic that is objectively measured and evaluated as an indicator of normal biological processes, pathogenetic processes, or pharmacologic responses to a therapeutic intervention."[2] Since that time the definition has been broadened to include not only the incidence and outcome of disease but also any "... laboratory measurement that reflects the activity of disease processes."[3] Extending this concept to imaging provides the definition of an MR biomarker as any *anatomic, physiologic, biochemical, or molecular parameter detectable with MR imaging methods used to help establish the presence and/or severity of disease*.[1] For RO, we have further refined this definition as *any anatomic, physiologic, biochemical, or molecular parameter detectable with MR imaging methods to identify the presence and/or severity of a malignancy and its response to therapy.*

Since the biomarker concept originated with drug development, much of the nomenclature describing them was taken from this perspective, as exemplified by Sorensen's four stages of biomarker development (Table I) where a given stage or term refers to a biomarker's overall utility. For the purposes of RO, Frank and Hargreaves[4] provide a more practical and relevant classification system dividing biomarkers into types 0, 1, and 2 as outlined in Table II. These three types (0, 1, and 2) are taken directly from the NIH Biomarkers and Surrogate Endpoint Working Group classification scheme for biomarkers and attempt to classify a biomarker in terms of its clinical impact or significance. Under this framework, Type 0 biomarkers demonstrate a correlation with a "gold standard" clinical assessor while a Type 2 reflect treatment efficacy validated through clinical trials.[4]

The majority of RO MR biomarkers described within this report will be considered as Type 0. It is important to note that Type 2 biomarkers are not true Type 2 (i.e., surrogate endpoint) since they have not been validated against the clinical outcomes for which they are being used.

3. BIOMARKER QUANTIFICATION

3.A. Quantitative descriptors

While many imaging biomarkers are capable of generating numeric values, this does not necessarily qualify them as being a quantitative imaging biomarker (QIB). Sullivan et al[6] described the characteristics an imaging biomarker must satisfy to be considered as a QIB. In particular, the value, or measurand, generated by the biomarker may be either a ratio variable or interval variable. Ratio variables have a clear definition of zero and the ratio of two given values can be interpreted. The measurement of tumor volume is an example in which a value of zero means the absence of the mass and where change in this value can be expressed as a percentage that is meaningful (i.e., ratio of two values). In contrast, interval variables do not have a meaningful zero, and while the difference between two given variables is meaningful, their ratio is not. A common example of this in CT imaging is measurement in Hounsfield units (HU). By definition, a measurement of zero based on the electron density and formalism of an HU is assigned to the density of water. A material with a HU of zero does not, in fact, have zero electron density. Furthermore, a material with a Hounsfield reading of 400, for example, is not twice the electron density of a material with a HU of 200. The difference between these two is meaningful in the sense that the 400 HU material has a higher electron density than the 200 HU material, but it is not twice the electron density. A clinical example of an interval variable is CT-based estimates of the percentage emphysema index and the percentile density in the assessment of emphysema severity.[6] Therefore, while the majority of MR biomarkers described in this work have some quantitative aspects, they are not necessarily, by definition, a QIB unless they can be defined as either a ratio or interval variable.

3.B. Standardized reporting efforts

With appropriate calibration, most imaging technologies can provide quantitative information about some properties of the material from which the imaging signal has emanated. Thus, imaging methods also constitute biomarker measurement processes and are conceptually similar to laboratory or physiological assays. Standardized terminology and methods have become established in medicine to describe, evaluate and validate laboratory assays. The same concepts and approaches should be applied to imaging assays. Although investigators in the imaging community have been active in developing and evaluating QIBs for several years, the development and implementation of QIBs has been hampered by the inconsistent or incorrect use of terminologies and methodologies pertaining to technical performance and associated statistical concepts.[6] Technical performance is an assessment of how a test performs on reference objects or subjects and under controlled conditions. Once technical performance is established for a given biomarker, additional research needs to be performed to determine clinical validation (how it performs in a human population, e.g., clinical

sensitivity and specificity) and clinical usefulness (its benefit in terms of clinical or regulatory outcomes).

In response to the need for reliable and reproducible quantification of biomedical imaging data, the Radiologic Society of North America (RSNA) in 2007 organized the Quantitative Imaging Biomarkers Alliance (QIBA) whose mission is to improve the value and practicality of quantitative imaging biomarkers by "*reducing variability across devices, patients and time*." (http://www.rsna.org/QIBA/) QIBA participants span a wide range of expertise including clinical practice, clinical research, physics, statistics, engineering, regulatory, pharmaceutical, and computer science.

Quantitative Imaging Biomarkers Alliance employs a systematic, consensus-driven approach to produce a QIBA Profile, which is a standard document that includes two items: (i) One or more claims, which tell a user what can be accomplished by following the Profile; and (ii) the specifications necessary to achieve that claim (i.e., specifications tell a vendor what must be implemented in their product, and tell a user what procedures are necessary during image acquisition and processing). QIBA Profiles are based on published data, when available and on expert consensus opinion for specifications where insufficient data exist. The focus of a profile is to reduce bias (accuracy) and improve reproducibility (precision) of a quantitative result from an imaging examination (see Section 3.C for further definition). The QIBA process specifies what to achieve, rather than how to achieve it, and the general approach is as follows:

1. Identify Sources of Error and Variation in Quantitative Results from Imaging Methods: Stakeholders identify problems leading to error or variability in quantitative results from imaging methods.
2. Specify Potential Solutions: Stakeholders identify potential strategies, infrastructure, or guidelines for error mitigation and collaborate on development of hardware, software, and protocol solutions.
3. Test Solutions: Vendors and researchers implement QIBA solutions (profiles) to assess their feasibility and efficacy.
4. Promulgate Solutions: Validated solutions (profiles) are disseminated and implemented through vendor adoption, research integration, and clinical education.

Quantitative Imaging Biomarkers Alliance also established a Metrology Working Group which developed recommendations on terminology and methodology for assessing the technical performance of a quantitative imaging biomarker. Publications from that group can be found at https://www.rsna.org/research/quantitative-imaging-biomarkers-alliance/metrology-papers.

QIBA provides an established framework for standardizing QIB development which can be applied to expedite the translation of a QIB through the biomarker development process. The adoption of the QIBA methodology for MR biomarker development in RO is supported and encouraged by the authors of this work. To demonstrate how the QIBA methodology can be adopted for QIB MR biomarkers, Appendix A.1 (Online Supplemental Material) uses the ADC as an illustrative example, describing the steps necessary for biomarker development within the QIBA framework.

3.C. Validation

Biomarker validation describes the process of characterizing a biomarker in terms of its measurement performance characteristics and establishes the range of conditions in which the biomarker's values are considered reproducible and accurate.[7] As such, all biomarkers require validation. The extent of the validation process will in turn determine the degree to which the biomarker can be used in diagnosis, prognosis, or as an indicator of therapy response. In the consensus statement on imaging biomarkers for cancer studies, O'Connor et al[8] provided guidance regarding the steps necessary to translate imaging biomarkers in cancer from discovery to surrogate endpoint. Thus, the methodology described in this work has been adapted to the application on MR biomarkers in RT. In order for a biomarker to be considered a surrogate, the ultimate and most effective use of a MR biomarker, it must pass through three domains in sequential order: discovery (Domain 1), validation (Domain 2), and qualification and ongoing technical validation (Domain 3). For the purposes of this report, the assumption is made that the MR biomarker has passed through Domain 1, having already been identified as a biomarker of cancer in RT. Once a potential biomarker has been discovered (i.e., passed through Domain 1), it must then be validated which involves biological and clinical validation and determination of clinical utility (Domain 2). If it successfully completes these steps it is precision and bias must be quantified (Domain 2). Successful transition through Domain 3 requires biomarker qualification. These steps are described as follows:

3.C.1. Biological validation, clinical validation, and clinical utility (Domain 2)

Biological validation refers to the linking of the biomarker to the source of its signal (i.e., the underlying normal or malignant biology). For the purpose of this work, the assumption is made that this link is known well enough to establish a sufficient understanding of the biological processes that generated the signal. As identified by O'Connor et al[8] an essential component of this stage involves animal studies to enable "clinically relevant imaging biomarkers to be related to fundamental biological processes that can only be measured with invasive techniques".[8] However, it is important to note that in many instances this exact relationship remains to be fully elucidated, particularly in terms of malignancy. Clinical validation involves the establishment of the relationship between the biomarker value and a clinical variable, such as a patient's performance status following therapy. Clinical utility is the demonstration that the biomarker leads to a net improvement in health outcomes or provides information on the diagnosis, treatment, management,

or prevention of disease.[8] In essence validation identifies how well the biomarker performs in a human population[6] while utility identifies the relationship with overall clinical outcome. The requirements for establishing clinical utility — a necessary step toward establishing the biomarker as a surrogate — are more demanding when compared to those clinical validation and involve the most rigorous testing, including multicenter prospective clinical trials with sufficiently large patient populations with long-term clinical follow-up to establish the appropriate statistical power.[9] Because of the expense and effort required to determine clinical utility, few imaging biomarkers have been established as surrogates. Most MR biomarkers are currently viewed as being correlated with clinical variables.

3.C.2. Precision (Domain 2)

O'Connor et al[8] described quantification of both repeatability (i.e., variance of repeated measures under the same conditions in the same individual) and reproducibility (i.e., variance of measurements performed on different equipment, by different operators, at different sites) as related parameters necessary to define the precision of the biomarker. For RO applications, assessment of these two parameters can be achieved through the establishment of a QIBA profile in which the precision of the biomarker is established, along with the conditions for which these values are valid including compliance with QIBA image acquisition and processing/analysis.

3.C.3. Bias (Domain 2)

Bias (accuracy) refers to the systematic difference between the measured and true value. Technical bias, the difference in measured vs known biomarker values when measured in a phantom, is easier to quantify than clinical bias, which requires assessment of the difference between the known vs measured value in patients. Again, the establishment of a QIBA profile with its associated protocol and claims is the most straightforward method for quantifying MR biomarker bias.

3.C.4. Qualification (Domain 3)

Qualification — the final process in biomarker development — refers to the establishment of the link between the underlying biological processes and clinical endpoints, thereby establishing the fitness of the biomarker for a given purpose, such as monitoring therapeutic response following RT. Similar to clinical utility, few MR imaging biomarkers reach this level of validation, and without it a biomarker cannot be used as a surrogate measure of the clinical outcome of interest. When evaluating biomarker qualification, considering the quality of the underlying validative clinical data is

TABLE III. Stepwise approach to MR biomarker development and testing in radiation therapy. Biomarker type includes integer values as described by Frank et al[4] as described in Table 2 while domain describes the respective sequential steps required for biomarker translation from discovery to surrogate as outlined in Section 3.C.[8]

Domain	Biomarker Type	Required Procedures	Step #	Comments
1	–	Determine if biomarker is quantitative and what type.	1	Determine if the biomarker is quantitative or not. If the biomarker is quantitative characterize the biomarker measurand is either a ratio variable or interval variable. See Section 3.A for details.
1	–	Identify underlying biological processes associated with the MR biomarker.	2	Biomarker cannot be used in any phase of the radiation therapy process. The potential application/use of biomarker can be investigated.
2	–	Biomarker validation.	3	Requires continued investigation of application/use of biomarker. No treatment decisions based on quantitative biomarker values can be made. See Section 3.C for details.
2	–	Development of vendor neutral quality control program and phantom.	4	Requires QC/QA procedures in order to benchmark quantitative biomarkers. QC/QA programs should be vendor agnostic thereby ensuring that similar biomarker values are obtained independent of scanner manufacturer.
2	–	Establish standardized imaging protocols.	5	Required before QIB data can be used. A single, standard imaging protocol should be developed which is independent of the specific model, make and hardware of the MR scanner. If not achievable a standard protocols for a given manufacturer and field strength should be developed to allow for longitudinal comparison of biomarker values so as to provide meaningful, quantitative interpretation of biomarker values.
2	–	Establish mathematical model(s) and standardize analysis techniques.	6	Necessary to allow for use of biomarker data across multiple sites and for comparison of QIB data.
2	0	Establish clinical validation.	7	Use of biomarker values can be incorporated into the radiation therapy process. Treatment decisions cannot be made based on MR biomarker information alone.
2	1	Establish clinical utility.	8	Biomarker can be used in the radiation therapy decision process. Until utility is established, it should not be used in the absence of established clinical variables.
3	2	Establish biomarker qualification.	9	May be used as a diagnostic biomarker of disease (prognostic), a method for directing therapy or as a surrogate endpoint of treatment response (predictive).

also important, since the given clinical study quality may be highly variable, ranging from a small retrospective series to larger, prospective, or randomized trials.

3.D. Development of MR biomarkers for use in radiation oncology

The appropriate use of an MR biomarker in RT depends on the matching of the biomarker type and domain to the application of the biomarker information. For example, only MR biomarkers that qualify as surrogate endpoints should be used to dictate treatment decisions or determine either response to therapy or treatment outcomes. Biomarkers that undergo thorough technical validation (Domain 2) but are yet to undergo qualification may still provide valuable, quantitative information that complements other known response measures. The progression of an MR biomarker along the translational pathway requires significant research and development as described by Abramson et al.[10] In addition, the ongoing evolution of QIBA biomarker profiles address many, if not all of the steps involved in the biomarker development process and is therefore a valuable resource to understanding the process. Table III provides a list of procedures and guidelines recommended to transition a biomarker from the discovery phase to surrogate endpoint, and in doing so provides an indicator of where the biomarker falls along this pathway. Unlike Tables I and II which classify a biomarker in terms of its development stage (initial = prebiomarker, final = licensed) and type (0, 1, and 2) Table III outlines in sequential order the steps that are necessary for a biomarker to progress from discovery to surrogate endpoint.

4. MR BIOMARKERS, ASSOCIATED BIOLOGIC AND GENETIC PROCESSES, AND IMAGING TECHNIQUES

MR biomarkers have been classified into two categories: those in active development and emergent. This classification is based on the status of a MR biomarker specific to RO as opposed to their overall development. Active development refers to the fact that the biomarker has been shown to correlate with disease identification and response to therapies related to oncology and that significant efforts are underway to further develop the biomarker specific to RO. Emergent indicates the parameter under consideration has been classified as a biomarker and that preliminary data exists indicating that the biomarker has potential application in RO.

4.A. MR biomarkers in active development

There are a number of MR biomarkers measuring gross anatomy down to the molecular features of tissue that are under active development. Many of these biomarkers have direct applicability to oncology imaging by providing information on disease location, extent, and response to therapy. These biomarkers are described below both in terms of the underlying biological processes that produce the biomarker signal, as well as their current and potential application(s) in RO.

4.A.1. Anatomic

MR-derived estimates of tumor volume provide a quantitative estimate of disease extent and burden as changes in tumor volume provide a method for determining response to therapy. As such, tumor volume has strong potential as a clinically useful QIB and is simple to measure. However, the diversity of contrast mechanisms for anatomical MR imaging, in addition to signal heterogeneity as a function of tumor type pose challenges in the clinical implementation of this biomarker. Even when accurate measures of tumor volume can be made which are known to be more problematic in MR due to spatial distortion from multiple effects, not all malignant masses demonstrate a strong correlation with treatment outcome. For example, within the lung it is generally appreciated that change in tumor volume reflect therapeutic response.[11] In contrast, in Ewing sarcoma — the second most common malignant bone in pediatrics and young adults — inadequate early change in tumor volume following chemotherapy is not predictive of adverse outcome while late volumetric change with histologic response was demonstrated to have higher correlation with event free survival.[12] With the increasing use of targeted and immunotherapies it is unclear what anatomic changes will occur and how well they correlate with response to therapy. Additional investigation is therefore required before this biomarker can be used as a surrogate endpoint (i.e., Type 2). There also is considerable variability in the results obtained when manual segmentation of tumor volumes is performed indicating that more robust and consistent processes such as the use of deformable image registration and automatic segmentation algorithms are required.

Quantification: In an attempt to measure changes in tumor size in oncology as a reflection of response to therapy, the Response Evaluation Criteria in Solid Tumors (RECIST)[13] was established in 2000. Since that time, a revised version, the RECIST 1.1, has been published.[14] RECIST 1.1 requires the identification of up to five target lesions within an organ, followed by measurement of either the longest (non-nodal lesion) or shortest (nodal lesion) dimension. A sum of diameters is then used as the baseline measurement. Response to therapy is determined based on defined percentage and absolute change in this value. While the guidelines provide a defined protocol for assessment of response, it does not reflect the entire tumor burden and the RECIST working group has recognized that true volumetric measurement would be preferred over unidimensional measurements if sufficient reproducibility of volume measurements was achievable. However, volume measurements are more sensitive and variable across observers when manual segmentation methods are used.[15]

As a biomarker of treatment response, either RECIST-derived or volumetric measurements can be considered as

Licensed and of Type 2, given that the absence of the physical dimensions of a mass is indicative of no disease or complete treatment response. As a QIB, either estimate can be considered as a ratio variable.

Anatomic QA/QC: The validity of either volumetric or RECIST-based estimates of tumor burden relies upon the spatial fidelity of the MR data from which they are derived. To this end, quality control programs developed by professional bodies, such as the American College of Radiology (ACR),[16] the American Association of Physicists in Medicine (AAPM),[17] and MR scanner manufacturers, exist to ensure that MR scanners produce images with the highest spatial fidelity possible. In addition, it is likely that a recently formed AAPM Task Group (TG # 284) entitled "Magnetic Resonance Imaging Simulation in Radiotherapy: Considerations for Clinical Implementation, Optimization, and Quality Assurance" will produce a report covering issues related to quality control of MR data, particularly in the setting of its use in RO. The quality assurance guidelines and tolerances recommended by the upcoming report should be followed. Furthermore, the MR images from which spatial measures of disease burden are obtained should comply with the following:

1. Performance of an established quality assurance program recommended by accrediting or professional bodies with specified tolerances over defined imaging volumes.
2. The use of either 2D or 3D gradient distortion correction algorithms for all MR data depending upon the acquisition method (2D vs 3D).
3. Avoidance of spatial measurements on sequences known to be prone to geometric distortions, such as single shot echo planar imaging (EPI) for DWI.

Anatomic measures as biomarkers in radiation oncology: Guidelines such as RECIST or Response Assessment in Neuro-Oncology criteria (RANO) provide categorical definitions based on 2D measurements for therapy response assessment using imaging and can be easily incorporated as such for therapy assessment. While the clinical implementation of these assessments is relatively widespread, both RECIST and RANO reports have recommended eventual transition to tumor volume measurements. Particularly for RO, as radiation treatment plans are based on tumor and treatment volumes defined in the treatment planning system, these segmented volumes tracked consistently over time would provide more sensitive measurements of tumor volume change.

Biomarker strengths, weaknesses, and limitations: As defined by the RECIST 1.1 criteria,[14] complete response to therapy is determined by the disappearance of visible tumor on post-treatment imaging. Beyond the situation of a complete response, the quantitative measurement of the relative changes in an enhancing tumor has limitations. The reliance of human measurement introduces a level of subjectivity and user-dependent variability regarding slice selection, visual edge detection, and identification of long or short axes. The use of one or two length measurements to represent tumor volume is also considered as a simplification of tumor volume, although protocols for volumetric measurements may be burdensome to perform and have not been standardized. For some tumors, change in tumor size is a late indicator of response. In addition, tumor volume changes also occur due to processes such as inflammation or necrosis and may not be reflective of tumor response to treatment.[18] Thus, guidelines are frequently modified for various disease sites or therapeutic approaches. Similarly, strategies incorporating active surveillance or targeting progression-free survival may not require the elimination of tumor mass as an endpoint, and thus must rely on other biomarkers to be effective.

4.A.2. Relaxometry

Tissue contrast in MR is determined by differences in relaxation rates of the MR signal following the addition of radio frequency (RF) energy.[19,20] Quantification of this effect and the differences across various tissues and organs is referred to as relaxometry, with the three most common relaxometry parameters being T_1, T_2, and T_2^*. T_1 represents the time constant characterizing so-called spin-lattice relaxation and relates the exchange of energy between the microstructure, historically referred to as the "lattice" (i.e., local atomic and molecular environment), and the ensemble nuclear magnet moments (i.e., spin system) of the tissue. T_2 relaxation, also known as spin–spin relaxation, is related to the inverse of the tumbling rate or correlation time (τ_c) of the molecule of interest. Because τ_c increases with decreasing molecular size and mobility of the molecule within the local microscopic environment, T_2 is positively associated with the relative mobility of molecules within tissue. Finally, T_2^* is a measure of both T_2 and macroscopic perturbations to the main magnetic field (i.e., B_0). These relaxation times are time constants of exponential decay or regrowth commonly expressed in milliseconds, while R_1, R_2, and R_2^* are their reciprocal rates expressed in 1/s or Hertz.

Since the inception of MR imaging, differences in tissue relaxation values have been thought to infer information regarding tissue organization and microstructure which can be used to diagnose and stage various benign and malignant diseases. These changes can be qualitatively assessed by means of imaging techniques that provide tissue contrast weighting based on a specific relaxation property (e.g., T_1- or T_2-weighted imaging) or quantitatively by means of parametric MR imaging of an individual relaxation parameter.[19]

Relaxometry quantification: MR relaxometry quantification involves the estimation of T_1, T_2, and T_2^*. Due to the

historically qualitative nature of MR imaging techniques and the variability among MR equipment, techniques and field strengths, standardization of quantitative in vivo MR relaxometry imaging is lacking. QIBA profiles for these relaxometry parameters do not exist and are not under development. Consequently, claims pertaining to measurable change in individual biomarker values and percentage confidence limits do not currently exist.

As a biomarker, relaxometry values can be considered as being at the *biomarker* stage of development as defined in Table I and classified as Type 1 (Table II) in which either the absolute value or its change is associated with disease stage. However, as a QIB, relaxometry values do not conform to either ratio or interval variable definitions. Although MR systems may estimate zero values for a given relaxometry parameter, this value reflects the sensitivity of the equipment as opposed to the presence of a true zero value. Similarly, the absence of a zero value could be a qualification for consideration as an interval variable; however, differences in relaxometry values do not scale proportionally to the associated physical parameter. For example, while T_2 is considered to be positively correlated with fluid content, a doubling of tissue T_2 in units of milliseconds does not reflect a doubling of tissue fluid content.

Relaxometry QA/QC: Recent collaborative efforts between the International Society of Magnetic Resonance in Medicine (ISMRM) and the US National Institute of Standards and Technology (NIST) has resulted in the development of a relaxometry phantom and standardized imaging protocols for quantifying T_1, T_2, and proton density (https://www.nist.gov/programs-projects/quantitative-mri). The phantom is a modified version of that developed for the Alzheimer's Disease Neuroimaging Initiative (ADNI). The phantom is spherical in shape with an inner diameter of 200 mm, filled with deionized water, and 57 fiducial spheres with inner diameters of 10 and 40 mm. The larger diameter spheres are used for quantitative T_1, T_2, and proton density assessment. Imaging of the phantom, using NIST scanning protocols, assesses the quantitative accuracy of these parameters and compares the reproducibility and variability of these values across MR scanner platforms.

Relaxometry as a biomarker in radiation oncology: In malignancy, both qualitative and quantitative changes can be indicative of the presence or activity of cancer cells, necrosis, radiation damage, inflammatory response, perfusion, and more. Quantitative relaxometry presents a challenge, although, in that precise quantification involves the use of imaging sequences that require long acquisition times obtained under ideal imaging conditions. As a result, in vivo approaches involve faster techniques, often by acquiring multiple acquisitions per repetition, such as multiple low flip angle gradient echo acquisitions after an inversion pulse for T_1, multiple spin echoes following an excitation pulse for spin echo T_2 measurements, or multiple gradient echoes for T_2*. Corrections for flip angle, RF inhomogeneity, slice profile, or even other relaxation times are often necessary and further decrease the precision of relaxometry measurement. As a result, qualitative descriptive terms such as hypo or hyper intense are used in the context of the type of tissue weighting. Practitioners are cautioned against establishing specific parameter values and ranges based on literature review alone due to the broad heterogeneity in these values resulting from a lack of standardized acquisition and image processing methods. Additionally, it should be noted that relaxometry values are field strength and temperature dependent.

Biomarker strengths, weaknesses, and limitations: Changes in T_1, T_2, and T_2* can be very sensitive to changes in tissue composition, function, temperature, pH as well as oxygenation but the lack of standardized quantitation limits the utility of quantitative measurements. Relaxometry is generally time-consuming; hence clinically feasible techniques will vary depending on time limitations or motion management strategies. While these techniques can often be verified or calibrated in a phantom, they can still present widely varying values in human and animal subjects. Additionally, different techniques have varying sensitivities to other factors, such as physical properties of the system and subject (e.g., B_0 or B_1 inhomogeneity), and tissue properties like temperature, diffusion, perfusion, and magnetization transfer. Relaxation values are also dependent on field strength in controlled laboratory settings. While general relationships are known, there has been little attempt to calibrate relaxation values for field strength, even for otherwise identical imaging environments. For in vivo imaging, the assumed monoexponential model of relaxation is a simplification of the magnetization in each voxel, since tissue will almost always contain mixed species, either by partial volumes of adjacent tissues or by mixed composition of chemical species within a voxel of similar tissue and that relaxation, particularly T_2 is characterized as a multiexponential rather than monoexponential decay over time.[21] Clinically, multiple biological processes can influence relaxation values, confounding the utility of absolute values. For example, since oxygenation can affect both T_2 and T_2*, patients under anesthesia breathing oxygen rich gases result in skewed values. For these reasons, quantitative relaxometry does not exhibit either the precision or accuracy to be considered as an oncologic QIB. However, it will continue to provide insight into both disease diagnosis and treatment monitoring as a qualitative biomarker and most likely be used in combination with other MR QIBs.

4.A.3. Spectroscopy

Magnetic resonance spectroscopy (MRS) describes the method of obtaining an MR signal from the nucleus of an atom which exhibits a net nuclear magnetic moment.[22] Due to its relative abundance within the human body, hydrogen (^{1}H) is the most common atomic species from which an MR spectroscopic signal is obtained. Spectroscopic signals from

other nuclei, such as ^{13}C, ^{19}F, ^{23}Na, and ^{31}P, can also be obtained[23] but are less frequently used due to their decreased natural abundance relative to hydrogen and resulting decreased SNR. Unlike proton MRI, proton MRS relies on the quantification of signals from hydrogen nuclei associated with molecules other than water, the most common of which include lactate, NAA, glutamine, glutamate, Cr, Cho and ethanolamine metabolites, citrate, polyamines, myo- and scyllo- inositol, carnosine, and lipids. Less frequently targeted metabolites include glutathione, taurine, 2-hydroxyglutarate (2-HG), gamma-aminobutyric acid (GABA), glycine, aspartate, taurine, succinate, tryptophan, alanine, glucose, and mannitol in brain, prostate, muscle, liver, and kidney.[24] Electron shielding unique to each molecule induces an alteration of the Larmor frequency of a molecule's hydrogen nuclei and is quantified in terms of frequency shift relative to tetramethylsilane. Typically measured in units of Hertz or parts per million (ppm), this shift is also known as the chemical shift and allows for different metabolites to be quantified in terms of the chemical shift of the metabolite in question. Because in vivo tissue contains many different chemical species, the signal obtained contains signals from all of these individual metabolites is referred to as a spectrum. As the MRS spectrum encodes signals from hydrogen within metabolites as opposed to water, MRS is generally considered to be a biomarker of metabolic or functional activity.

Since the biochemical environment of tissue is dramatically altered in malignancy,[25-27] MRS, or clinically MRSI, has the potential to be a sensitive biomarker of disease type, stage, and aggressiveness[25-27] and has been reported to predict the efficacy of therapies including chemotherapy[25,27,28] and radiation.[29-31] Challenges include the relatively low SNR of the MRS signal due to the significantly decreased amount of hydrogen in metabolites compared to water (~ 110 Molar vs ~1–10 milliMolar) and the need for a highly uniform B_0 field. Historically, these differences have been overcome by performing MRS within a relatively large single voxel in an organ or tumor in which the B_0 field can be effectively shimmed, such as the brain or prostate.[32] Obtaining multiple signal averages, typically resulting in relatively low spatial resolution of the acquired spectrum and long acquisition times, is helpful, as well. Spectra derived from a single voxel is typically referred to a single voxel spectroscopy but can be extended to include spectra from multiple voxels by effectively performing phase encoding of an individual voxel, producing a so-called MRSI.[23]

Biomarker quantification: The concentration of a given metabolite (C_M) within the voxel of tissue under interrogation can be derived from the MRS spectrum according to the relationship $C_M = \frac{A_M}{K_G V_B}$ where A_M is integrated signal amplitude or area under the curve of the metabolite M peak, K_G a "global" constant of proportionality, and V_B the volume of the voxel.[33] While simplistic in its formulation, absolute quantification of a given metabolite's concentration is challenging due to the complex dependence of K_G on many interrelated factors.[33] As such, quantitative assessment of in vivo MRS spectra typically involves the normalization of spectral peaks by dividing the spectral profile (signal intensity) by the peak value of a reference metabolite such as NAA. Additional processing of spectral information and curve fitting is routinely performed to improve the fidelity of the spectra. While there are multiple approaches to curve fitting spectra in both the time and frequency domains,[24] one of the most common is known as the linear combination model (LCModel).[22]

Several methods exist for the quantitative analysis and reporting of ^1H metabolites derived from in vivo MRS/MRSI spectra. One such approach involves using the main peak area ratio of Cho and NAA from three-dimensional (3D) MRSI taken from glioma patients using normal brain voxels as internal controls for quantifying the probability of abnormality at each voxel location (i.e., a quantitative abnormality index).[34] Another approach developed for ^1H MRSI of the prostate involves calculation of the (Cho + polyamine + Cr)/citrate ratio. Historically referred to as the (Cho + Cr)/citrate ratio or CC/C ratio, it is based on the fact that in spectra taken from regions of prostate cancer the citrate and polyamines are significantly reduced or absent, while the total-Cho resonance is elevated relative to spectra taken from surrounding healthy, peripheral zone tissue.

MRS-derived absolute or relative metabolite concentration can be considered a Type 1 biomarker given that MRS has been shown to identify malignancies in a range of organs and is predictive of therapeutic intervention.[25-31] Additionally, MRS-derived concentrations can be considered ratio variables, since zero theoretically indicates the absence of a given metabolite and a multiplicative increase or decrease in the value indicates a proportional increase or decrease in the concentration of the metabolite in question. As ratio variables, MRS-derived concentrations qualify as a QIB. In the absence of an MRS or MRSI QIBA profile and associated claims, generalized statements regarding reproducibility and quantitative change in MRS/MRSI associated with disease extent and /or therapeutic response cannot be made.

Spectroscopy QA/QC: To date, a uniform QA/QC program including phantoms and standardized protocols for performing MRS and MRSI does not exist, although several authors and groups have attempted to address this deficiency. For example, a report published by AAPM task group #9 provided recommendations for performing MRS in the brain,[35] while Hunjan et al[36] have provided both a phantom and analysis protocol for quality assurance in MRSI. Although MR scanner manufacturers who offer MRS and MRSI capabilities typically provide a metabolite phantom and testing protocol, significant variability exists among vendors. Due to the absence of a QIBA related QA program and industry accepted phantoms and protocols, it is recommended that individual facilities develop and implement their own QA program. As a guide, the interested reader should refer to the

recently published consensus statement on MRS in the brain which includes general QC recommendations.[37]

Spectroscopy as a biomarker in radiation oncology: Given that MRS and MRSI provide a noninvasive method for quantifying the metabolic state of tissue, and that cancer is known to fundamentally alter tissue metabolic homeostasis, both techniques have significant application in RO. In addition, it is generally appreciated that therapy-induced metabolic changes in tumors precede anatomical changes. While they can be applied to any tissue and organ, both approaches are used most frequently in the prostate and brain.

Prostate: In the prostate the CC/C ratio is one of the most widely used quantitative metabolic biomarkers for detecting cancer and has been used in the majority of the current ≈ 320 publications on prostate MRI/MRSI.[38] In a single study it was demonstrated that when the CC/C ratio is ≥ 3 standard deviations above the normal value, there is minimal overlap between spectroscopic voxels from regions of cancer and healthy peripheral zone tissues.[39] The magnitude of elevation of the CC/C ratio has shown a correlation with cancer grade.[40-42] The addition of the CC/C ratio and T_2-weighted MRI to standard clinical nomograms improved the prediction of indolent vs aggressive prostate cancer at the time of biopsy diagnosis[43] and radiation treatment planning.[44-46]

Staging by MRI/^{1}H MRSI at diagnosis has been found to be of incremental prognostic significance in patients with moderate and high-risk prostate tumors going on for radiation therapy.[47] McKenna et al noted that the finding of more than 5 mm of extracapsular extension prior to radiation seems to be of particular negative prognostic significance, and the latter group may be candidates for more aggressive supplemental therapy.[48] Several studies of prostate cancer patients have directly integrated MRI/MRSI data into the radiation treatment plan in order to optimize radiation dose selectively to regions of prostate cancer using either intensity-modulated radiotherapy (IMRT)[49-51] or brachytherapy[52-55]; however, this is not being done in routine clinical practice.

Local recurrence of prostate cancer after RT is currently dependent on histopathology obtained from transrectal ultrasound (TRUS) — guided prostate biopsies. However, 37% to 50% of cancers can be isoechoic or only slightly hypoechoic on TRUS leading to false negative rates of up to 30%.[56] Combined MRI/MRSI allows for an assessment of the entire prostate thereby overcoming the sampling errors of TRUS guided biopsies. Imaging and PSA management after radiation treatment requires a long time to determine response with an expected PSA nadir at up to 24 months after completion of radiation.[57-59] Although conventional T_2-weighted MR imaging of the treated prostate is limited by the post-treatment loss of zonal anatomy and diffuse low signal, studies have demonstrated the ability of ^{1}H MRSI to discriminate residual or recurrent prostate cancer from residual benign tissue and atrophic/necrotic tissue after RT.[30,60,61] These studies have relied on elevated Cho to Cr ratio as an indicator of residual/recurrent prostate cancer since polyamines and citrate disappear early after therapy in both residual healthy and malignant tissues. Two published MRI/MRSI studies demonstrated that three or more consecutive voxels having Cho/Cr >1.5 resulted in the ability to predict the presence of cancer after RT with an accuracy of ≈80%.[29,30] Moreover, the addition of ^{1}H MRSI to T_2-weighted MR imaging (area under the curve (AUC) = 0.79) was shown to significantly improve the diagnostic accuracy of T_2-weighted MR imaging alone (AUC = 0.67) in the detection of locally recurrent prostate cancer after definitive external beam RT.[30] Incorporation of ^{1}H MRSI to T_2 weighted (AUC = 0.84) and/or DWI (AUC = 0.86) significantly improved the assessment of patients with suspected recurrence after radiotherapy, and a combined approach with all three modalities (AUC = 0.87) may have the best diagnostic performance.[62]

Brain: Quantitative analysis of metabolite concentrations within the brain have identified a Cho-containing compound-N-acetylaspartate index (CNI) threshold of 2.5 to distinguish tumor from normal, edematous, gliotic, and necrotic brain tissue with high sensitivity (90%) and specificity (86%).[63] Additionally, this threshold has been used to improve surgical,[64] radiation and combined radiation/ chemo/therapy/ antiangiogenic treatment planning.[65,66]

For radiation treatment planning and in monitoring treatment response, multimodality studies that include ^{1}H MRSI to indicate metabolic activity from tCho levels and MRI measures of perfusion may help with the targeting of biopsies to areas of maximum abnormality, thereby improving diagnosis and subsequent RT and outcome assessment.[31] In particular, data support their role in terms of both target delineation and response assessment.

Target delineation: Glioblastomas often infiltrate beyond the contrast enhancing region on MRI, and metabolic abnormalities have been shown to protrude beyond areas of lesion-associated T_2 hyperintensity, resulting in metabolically active disease detected on MRSI falling outside the high dose volume in a substantial proportion of patients.[67] In one study, patients with tumor-like MRS outside the 50% dose contour as determined using MRI had shorter time to treatment failure than those in whom the 50% dose contour included most of the tumor.[68] A prospective trial in patients with glioblastoma wherein MRSI was used to determine areas of high risk to augment the guidance of additional stereotactic radiosurgery found that patient survival was better than historical controls with standard conformal radiotherapy.[69] In addition to assessing the metabolic characteristics of tumor, 3D MRSI has also been used to assess tissue damage due to whole-brain radiotherapy.[70]

Response assessment: Metabolite changes observed in response to radiotherapy include a reduced tCho and increased lactate and/or lipid levels, consistent with a reduced number of viable tumor cells and increased hypoxia and necrosis. tCho/tCr and tCho/NAA have shown greater and more rapid alterations with time than changes in volume by

MRI, suggesting that MRS may be a more sensitive measure to assess treatment response and prognosis.[71] A greater than 40% reduction in the tCho of a lesion within the first 4 weeks of radiotherapy treatment has been associated with a 20-month progression-free survival compared to 9 months for a smaller tCho change.[72] An increase in tumor lipids after radiotherapy was predictive of an early treatment response and a better outcome in the case of malignant gliomas.[73] In another study, patients with higher lipid and lactate, or with larger abnormal tissue volumes as determined by CNI, had a worse outcome after treatment with chemo- and radiotherapy.[28] In pediatric supratentorial pilocytic astrocytomas, decreased mIns, indicative of tumor progression, preceded MRI changes.[74] Additionally, an increased tCho/NAA ratio was associated with treatment failure in diffuse pontine glioma, a pediatric tumor difficult to assess with conventional MRI.[75] At 1.5 T, an AUC of 0.926 was achieved using the tCho/NAA ratio to detect recurrence of primary tumors postradiation treatment.[76] ^{1}H MRSI at 3 T appears to provide greater sensitivity and has distinguished malignant glioma recurrence from post-treatment effects with an AUC > 0.9 based on tCho/tCr and tCho/NAA ratios: dynamic susceptibility contrast (DSC) MRI exhibited similar performance but diffusion-weighted MRI (DWI) was inferior.[77] tCho, lipid, and lactate are clearly important radiation response MRS markers, but the specific metabolite changes observed depends on the combination of tumor type and treatment, requiring that MRS biomarkers be developed and assessed individually. Additionally, the mixed nature of tissue (i.e., normal brain, necrosis, and gliosis) postradiation treatment makes accurate detection of recurrence a challenge; therefore, a multimodal approach is best to use in clinical practice.[77]

Biomarker strengths, weaknesses, and limitations: The noninvasive and quantitative nature of MRS/MRSI makes it a good endpoint for use in clinical trials of drugs or other clinical interventions. In longitudinal studies, MRS/MRSI can be performed repeatedly with no harmful consequence to the patient or the clinical target, unlike invasive measures such as biopsy. MRS data are sensitive to the effects of therapy that can be readily compared and correlated with other clinical measures.

Significant published patient data exists indicating that ^{1}H MRS/MRSI biomarkers could improve radiation treatment planning and treatment response monitoring.[38,43,55,60,67-69,72,76,78-84] Currently, although, ^{1}H MRS/MRSI biomarkers are not routinely used for RT treatment decisions, primarily due to the inability to fully combine the MRS/MRSI data acquired in published studies to validate them for clinical use. Validation is hampered by the significant heterogeneity in data collection, analysis and presentation between studies, which is in part due to a lack of consensus concerning data acquisition methods, processing protocols, output formats, and established quality assurance programs. This therefore identifies the need for improved standardization of methodologies and analysis such as those promulgated by QIBA. A study intended to demonstrate diagnostic accuracy of a novel method such as MRS should follow the 25 criteria set out in the Standards for Reporting of Diagnostic Accuracy (STARD) initiative.[85] Historically, very few published clinical MRS studies were designed to adhere to such criteria, or even to be formal clinical trials. Furthermore, most were performed at a single center on a small number of patients and thereby lacked statistical power. When formal meta-analyses of the clinical MRS/MRSI literature were performed,[86] few of the thousands of published papers qualified for analysis; those that met the evidence-based medicine (EBM) criteria had often been performed on small groups of patients or with earlier generation instruments. Consequently, the apparent poor performance of MRS on the meta-analysis resulted in the denial of reimbursement for MRS within the United States,[86] which highlights the importance of standardization to demonstrate the clinical value of all imaging biomarkers.

4.A.4. Diffusion and diffusion tensor

MR imaging sequences can be sensitized to the motion of water within tissue, providing insight into tissue microstructure in normal and disease states. In its simplest form, scalar diffusion information can be encoded using DWI techniques in which the overall diffusion of water within a voxel is encoded. More complex acquisition schemes can also quantify the diffusion tensor thereby providing vector information and is commonly referred to as diffusion tensor imaging (DTI).[19]

Encoding of the diffusion of water molecules is achieved by adding paired diffusion-encoding gradients to a conventional MR image acquisition scheme, such as a spin echo-echo planar imaging (SE-EPI) sequence. In SE-EPI sequences, a diffusion-encoding gradient is added before and after the 180 refocusing RF pulse in which the two diffusion-encoding gradients have the same first gradient moment. For bound water in which diffusion is highly restrictive (e.g., intracellular water), the nuclear spin of the hydrogen nuclei will experience phase accumulations caused by the two diffusion-encoding gradients that cancel and therefore will not alter the acquired MR signal. In contrast, the nuclear spins of hydrogen in unbound water that experience diffusion will accumulate a net nonzero phase between the first and second diffusion-encoding gradients. Since moving spins are no longer in phase with static spins within a voxel, the MRI signal drops because of complex addition. This difference can be quantified by the equation $S = S_0 e^{-b \bullet ADC}$ where S is the signal acquired within a voxel in the presence of diffusion gradient fields, S_0 is the signal in their absence, b is the b-value which is a function of the size, shape, and timing of the diffusion gradient field wave forms, and ADC is the apparent diffusion coefficient. Note that the ADC differs from the true diffusion value, as it represents diffusion averaged over all spatial directions. DTI is an extension of DWI in which specific diffusion directions are encoded independently, providing specific values of the diffusion tensor and in doing so, provides directional (i.e., vector) information on diffusion. While

DTI acquisitions are longer than DWI imaging, the diffusion tensor can be used as input data into postprocessing applications to create tractography images. The DTI data can also be used to generate spatial anisotropy parameters of diffusion such as the relative and fractional anisotropy (FA), which are not encoded using DWI techniques.[87,88] FA is given by the equation $FA = \sqrt{\frac{(\lambda_1 - MD)^2 + (\lambda_2 - MD)^2 (\lambda_3 - MD)^2}{2\left(\lambda_1^2 + \lambda_2^2 + \lambda_3^2\right)}}$ where MD (mean diffusion) is the trace of the tensor divided by 3 and λ is the diffusion eigenvalue along a given direction is the most commonly used measure of diffusion anisotropy due to the relative simplicity of calculation, the fact that it is rotationally invariant and sensitive to a broad spectrum of pathologies.[89] However, the scalar nature of this value means that it does not describe the tensor shape or distribution of diffusion.[89]

Diffusion quantification: A draft QIBA profile for DWI has been generated which includes claims related to DWI imaging in the brain, liver, and prostate. Specifically, that a measured change in the ADC of 11%, 26%, and 47% or larger in the brain, liver, and prostate, respectively, indicates that a true change has occurred with 95% confidence (http://qibawiki.rsna.org/images/7/7e/QIBADWIProfile_as_of_2019-Feb-05.pdf). Given that zero diffusion is possible, albeit improbable, DWI derived estimates of diffusion can be considered as a ratio variable of Type 0. The biomarker could also be considered as a Type 1 as diffusion is known to be altered in both benign and malignant masses and is used routinely to monitor response to therapy as described below.

Diffusion QA/QC: The QIBA DWI profile recommends performing quality assurance procedures that are generally accepted for routine clinical imaging of the MR scanner. In addition, quality assurance of DWI derived ADC values can be assessed using a QIBA DWI phantom[90] constructed in-house using QIBA recommendations or purchased commercially (High Precision Devices, Boulder, CO). The QIBA profile allows quantification of the ADC of pure water at a temperature of 0°C by assessment of ADC bias, error, and short- and long-term repeatability. For both DTI and DT tractography, a single standardized approach for QC and QA such as a QIBA profile does not exist. However, several QC/QA programs are currently available.[91] The need for a single standardized approach is recognized.[91]

Diffusion as a biomarker in radiation oncology: In many respects the ADC is well suited as an oncologic biomarker since it can identify and differentiate a variety tissues: benign from malignant masses, areas of necrosis vs abscess, true vs pseudo response/progression, and treatment response vs recurrence. Additionally, ADC does this in multiple sites, including the brain, head and neck, thorax, pancreas, bowel, genito-urinary, and musculoskeletal system.[92] In malignancy, increased cellularity and biological aggressiveness mean that the ADC will be less than in normal tissue due to increased tumor cell density.[93,94] In a recent recurrence pattern and survival outcome analysis study, Elson et al showed that for patients with glioblastoma multiforme (GBM), recurrence overlapped with preradiotherapy ADC hypointensity in 88% of cases,[95] clearly demonstrating the potential of using ADC

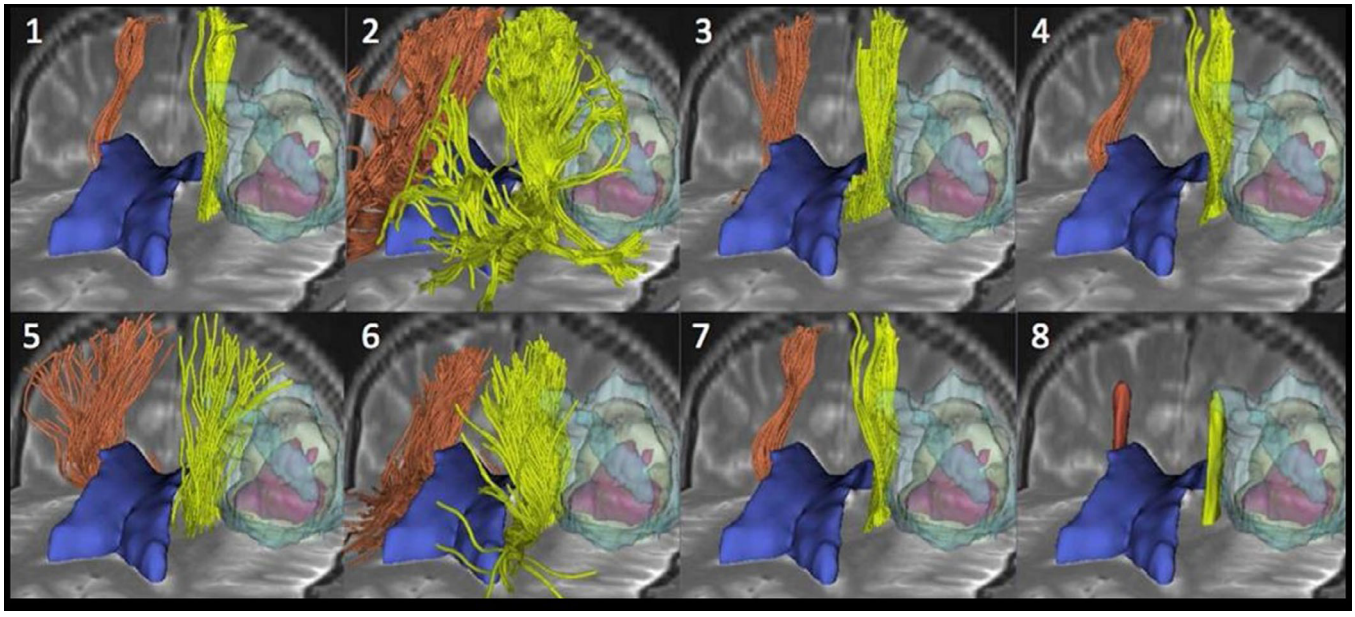

FIG. 1. Tractogram images created from a single DTI data of a patient with an anaplastic oligoastrocytoma grade III in which the eight images are generated by eight separate groups using three different algorithms. The tumor side and contralateral tracts are shown in yellow and orange, respectively. Tumor is shown in light yellow, necrosis in pink, and edema in bright blue. The ventricles are depicted in dark blue. The 3D data are superimposed onto a T_2-weighted anatomic image. Reproduced from[99] with permission. [Color figure can be viewed at wileyonlinelibrary.com]

to identify high-risk regions of the tumor for dose escalation. It also has the potential to differentiate cytotoxic from vasogenic edema in diffuse axonal injury.[96,97]

Biomarker strengths, weaknesses, and limitations: While the ADC and diffusion tensor related quantitative parameters, such as fractional anisotropy, are clearly promising oncologic biomarkers, they should not be used independently for making treatment planning decisions, such as determining overall tumor volume or therapeutic response, or differentiating necrosis from active disease within a lesion, etc. This is reflected in the QIBA profile that reports on percent change of the ADC indicating a 95% probability of a real difference in *only* three organs. Care should also be exhibited when comparing ADC values obtained using different pulse sequences and approaches, as the absolute ADC is dependent upon the b-values used.[98] In addition, much caution must be exhibited when using information derived from DTI data like tractograms. To illustrate this Figure 1 has been reproduced from the work of Pujol et al,[99] who enlisted eight international teams from leading academic centers to process brain tractogram data from four patient data sets using multiple processing algorithms. The figure demonstrates that, even with the same input data, there is significant variability between algorithms and operators, indicating as the authors noted that "DTI tractography suffers from a lack of standardization and the validity of tractography findings for neurosurgical decision making needs to be fully established."[99] Such cautionary advice can be applied equally to the use of these data in RT.

4.A.5. Perfusion

The delivery of metabolic substrates to and the removal of waste products from tissue are achieved by their perfusion into and out of the circulatory and lymphatic systems. In cancer, perfusion is altered across a range of malignant processes[100] and is therefore a powerful biomarker of disease stage, type, and therapeutic response.

MR imaging of tissue perfusion is achieved by the rapid imaging of either an endogenous or exogenous contrast agent into and out of a volume of tissue. Endogenous approaches involve the modification (i.e., preparation) of the magnetization of arterial blood flowing into the volume and comparing signal intensity changes without the magnetization preparation. Exogenous approaches involve the administration of a paramagnetic contrast (see Supplemental Material Appendix A1 for a full description of contrast agents) agent followed by visualization of the signal increase or decrease resulting from the perfusion of the agent in combination with the acquisition technique into and out of the imaging volume. Exogenous approaches fall into two main categories based on their acquisition schemes: Dynamic susceptibility contrast (DSC) and dynamic contrast-enhanced (DCE) imaging. Endogenous approaches are described by the method known as arterial spin labeling (ASL). The major acquisition schemes for both endogenous and exogenous approaches are as follows.

DSC Perfusion: DSC relies on the rapid imaging of susceptibility-induced signal loss resulting from the influx of a paramagnetic contrast agent through the microvasculature.[101,102] In regions of intact blood-tissue barrier, the contrast agent remains compartmentalized to the vasculature, where it creates a susceptibility difference between intravascular and extravascular spaces. The susceptibility differences result in microscopic field gradients that extend radially from the vessel, with the magnitude of the gradients dependent on the size of the vessel. In regions of larger vessels, local field inhomogeneities produced by the microscopic gradients result in phase accumulation of magnetized tissue. Both gradient and spin echo imaging approaches are used and provide contrasts that emphasize different populations of vessels. Gradient echo sequences are sensitive to all vessel diameters; spin echo sequences are sensitive to small vessel diameters (i.e., microvessels).[103]

DCE Perfusion: In DCE MRI, imaging of a paramagnetic contrast agent using an ultrafast gradient echo imaging sequence is performed. The inherent T1-weighted nature of the gradient echo sequence, in combination with the paramagnetic exogenous contrast agent, results in signal enhancement proportional to the concentration of the agent within the tissue. Unlike DSC, which relies upon an intact microvasculature, DCE relies upon the extravasation of paramagnetic contrast agent from the intravascular space to the extravascular, extracellular space (EES), occurring in regions of blood-tissue barrier disruption. Through dipolar interactions, the extravasated contrast agent results, predominately, in signal enhancement through T_1 shortening of tissue within the EES.

ASL Perfusion: ASL is a noninvasive method characterized by the use of magnetically labeled arterial blood water as an endogenous tracer.[104-107] The fundamental operation of most existing ASL methods is to produce two sets of images: a flow-sensitive "tag" image and a "control" image. Ideally, these images would differ only by the signal from inflowing blood, and their static tissue signals would be identical. The ASL signal — determined by the difference of the control and tag images — provides a qualitative estimate of perfusion. However, the ASL signal, which is derived from the difference between the tag and control images is only about 1% of either the tag or control image signal. Therefore, a time series of interleaved tag and control images is acquired to increase the ASL SNR. In addition, static tissue signal is often nulled with background suppression pulses. Although a multitude of labeling strategies exists, velocity-driven adiabatic fast passage using a train of low flip angle pulses in combination with a gradient along the flow direction (i.e.,

TABLE IV. Brain perfusion MRI biomarkers and commonly used acquisition strategies. GRASE = Gradient And Spin Echo. *Additional perfusion parameters can be obtained with each perfusion MRI method.

MRI Technique	Inherent Biomarker*	Unit of Measurement	Biomarker Type	Associated Biological Process	Common Acquisition Strategies
Dynamic Susceptibility Contrast (DSC)	rCBV	none	Ratio variable	Angiogenesis	2D single-shot gradient recalled or spin-echo EPI
Dynamic Contrast Enhanced (DCE)	K^{trans}	mL/g/min	Interval variable	Vascular permeability	3D spoiled gradient recalled echo
Arterial Spin Labeling (ASL)	CBF	ml/100g/min	Ratio variable	Hypo-perfusion	3D GRASE or Stack of Spirals

pseudo-continuous ASL) is the most widely accepted approach.

Perfusion quantification: A variety of perfusion related biomarkers that are either absolute or relative can be obtained depending upon the imaging method used. In DSC, indicator dilution analysis of the contrast wash-in wash-out (i.e., kinetic curves) can be used to estimate the ratio variable cerebral blood volume on a voxel-by-voxel basis. Since estimates of local hematocrit and determination of local arterial input functions are difficult to measure in vivo, although, relative cerebral blood volume (rCBV) is reported in most cases and has been shown to be a marker of angiogenesis and glioma grade.[108-111] In DCE, pharmacokinetic analysis of contrast-induced signal enhancement vs time, along with a baseline T_1 map of the tissue under interrogation, can be used to estimate the interval variable known as the vasculature-extravascular extracellular space transfer constant (K^{trans}) which is the rate at which contrast agent extravagates from the intravascular space to EES, on a voxel-by-voxel basis. Finally, the ASL signal, along with an estimate of the equilibrium magnetization within a voxel and an estimate of the T_1 of blood, can be used to estimate the ratio variable, cerebral blood flow (CBF) on a voxel-by-voxel basis. Biomarkers of perfusion are most commonly used in the brain. Table IV provides a summary of the common brain perfusion MRI techniques, along with their corresponding biomarkers, biological processes, and common acquisition strategies. As with QIB, perfusion derived parameters can be considered ratio variables of Type 1. For additional information on techniques, modeling and quantification of perfusion biomarkers, the interested reader is referred to the review article by Jahng et al.[112]

At the time of writing, QIBA has established a biomarker committee focused on perfusion, diffusion, and flow MRI (PDF-MRI) and has published a preliminary profile for DCE MRI. The profile includes a single claim pertaining to K^{trans} and the blood-normalized area-under-the-gadolinium-concentration curve ($IAUGC_{BN}$). The claim states that both K^{trans} and $IAUGC_{BN}$ can be measured from DCE-MRI data obtained at 1.5 T using low-molecular-weight extracellular gadolinium-based contrast agents with a 20% within-subject coefficient of variation for solid tumors at least 2 cm in diameter.

Perfusion QA/QC: To assist in quantitative QA, the QIBA DCE-MRI technical committee designed a phantom based on the ADNI Magphan phantom (The Phantom Lab, Greenwich,

TABLE V. General and radiotherapy specific QA considerations for MR perfusion techniques beyond the QIBA DCE-MRI protocol.

Perfusion Technique	General Considerations	Radiotherapy Considerations
DSC	● Prevent signal saturation of contrast bolus ● Ensure adequate temporal resolution for assessment of arterial input function ● Compact injection of bolus (~ 3cc/sec)	● Minimize spatial distortion arising from EPI-based acquisition schemes ● Minimize susceptibility induced distortions ● Ensure 3D gradient distortion corrections applied to DSC kinetic time series or resulting parameter maps
DCE	● Prevent signal saturation and adequate sampling of arterial input function ● Assess temporal stability of acquisition scheme ● Assess linearity of contrast agent versus concentration	● Minimize chemical shift and susceptibility induced distortions ● Ensure 3D gradient distortion corrections applied to DSC kinetic time series or resulting parameter maps
ASL	● Minimize T_2* effects ● Appropriate tagging plane selection to ensure tagging of arterial blood only	● Increase acquisition times to compensate for loss in SNR due to imaging in radiation therapy treatment position ● Ensure 3D gradient distortion corrections applied to CBF parametric maps

NY), in which quantitative T_1 estimates can be derived and compared to their known values.[113] Due to the narrow scope of the QIBA profile, there are several unmet QA needs, both in general terms, as well as related to the use of perfusion information in RT applications. Additional general and radiotherapy specific quality assurance considerations for DSC, DCE, and ASL are listed in Table V. It is also important to note that DCE is prone to specific artifacts and limitations related to a variety of factors including technique, postprocessing, and B_0 and RF field homogeneity considerations.

Perfusion as a biomarker in radiation oncology: Perfusion biomarkers can reveal insight into the state of tumor hypoxia and are therefore important parameters for radiotherapy.[114] Radiation therapy typically results in endothelial cell damage and small-vessel injury, decreasing capillary perfusion and tissue microvascular density. Perfusion biomarkers can be used for target delineation, assessment of treatment response, evaluation of normal tissue injury, and differentiation of true disease progression vs pseudo-progression. Of the perfusion MRI techniques previously discussed, DCE-MRI has been used most extensively, followed by DSC-MRI, and then ASL-MRI.

Since malignant masses exhibit characteristics that can result in an increase (via neovascularity or angiogenesis[115]) or decrease (via necrosis and hypoxia) in perfusion, quantification of this parameter can potentially serve as a powerful diagnostic and therapeutic oncologic biomarker. An increased perfusion rate as quantified by K^{trans} with respect to the background tissue is associated with a more aggressive tumor. Prostate cancer is illustrative of this effect in which an increase in K^{trans} has been observed in high grade compared to lower grade tumors and is presumed to be due to vascular hyper-permeability and consistent with increased expression of Vegf.[116] This parameter has a sensitivity and specificity comparable to PET/CT[117] and localizes cancer better than T_2-weighted MR imaging alone.[118,119]

Biomarker strengths, weaknesses, and limitations: The use of an EPI sequence can result in local (e.g., proximal to resection cavities, surgical clips, staples, etc), as well as global (stretching along phase encode direction) geometric distortions. Geometric distortion of DCE-MRI derived parameter maps (K^{trans}, etc) not only complicates tumor delineation, but also the coregistration of these maps to the anatomical image data used for treatment planning. In addition, susceptibility-induced signal dropout can result around resection cavities, which may limit the utility of DSC parameter estimates for radiotherapy. Although DSC-MRI is a robust technique, signal dropout near resection cavities limits its utility for delineation in the CNS.

Tumor perfusion related quantitative parameters are some of the most studied oncologic MR biomarkers, but multiple challenges remain, although, before they can be used in RO without the need for other markers. These include the lack of standardization regarding image acquisition, contrast agent administration, image processing, parameter quantification methods, and statistical analysis, resulting in significant variability in perfusion-derived parameters, such as within-subject variations of K^{trans} and the plasma space fractional volume as high as 59% and 0.82, respectively.[120] A major source of this variation is related to estimation of modeling parameters and the analysis model used.[121] Additional variation is also introduced as a result of errors in estimating the arterial/venous input function and the use of population-based estimates of the time delay between plasma and tissue contrast agent concentration change.[122] T_2* induced signal decay[123] is also subject to individual variations as well as differences between animal and human models.[124] In terms of modeling, sources of variability include omission of incomplete water exchange between the vascular and extravascular compartments,[112] inaccuracies in estimation of the plasma transit time,[112] and low temporal resolution of sampled points.[125] Standardization of acquisition, phantoms, analysis, and modeling will be necessary to minimize the aforementioned variability in diffusion-derived biomarkers. In addition to the QIBA perfusion profile under development at the time of writing, other standardization efforts include four workgroups established by the NIH Quantitative Imaging Network (https://imaging.cancer.gov/programs_resources/specialized_initiatives/qin/about/default.htm) focusing on phantom studies and QA, longitudinal studies, and database development and sharing. There is also the ACRIN standard DCE-MRI protocols and concepts reviewed by the Cancer Imaging Program, National Cancer Institute Steering Committee. Finally, integration of perfusion-derived biomarkers into the RO treatment planning process, such as the delineation of tumor target or use in graded dose planning, will require accurate knowledge of the threshold biomarker values to distinguish tumor and normal tissue, as well as quantification of the correlation of biomarker values and tumor aggressiveness, which will require pathophysiological validation. Since pathophysiological sample is difficult to obtain, few research studies have been performed in this arena.[126]

4.A.6. Blood oxygen-level dependent (BOLD) imaging

BOLD imaging relies on susceptibility-induced MR signal differences between oxy- and deoxyhemoglobin arising from neuronal activation within the brain.[127,128] This is a well-documented treatment-oriented model[129,130] based on the theory that metabolic activity from task-related brain activation (active state) results in coupled vascular activity. The vascular response following neuronal activation brings in oxygenated blood, thereby lowering the concentration of deoxygenated blood in the activated area. Since deoxygenated blood is paramagnetic while oxygenated blood is diamagnetic, the influx of oxygenated blood results in an increase in the MR signal when imaged with T_2*-weighted MRI. The signal increase is slight and field strength dependent, which is on the order of 1%–3% at 1.5 T and 3%–5% at 3 T, due to higher SNR and more pronounced T_2* effects. In order to extract these small

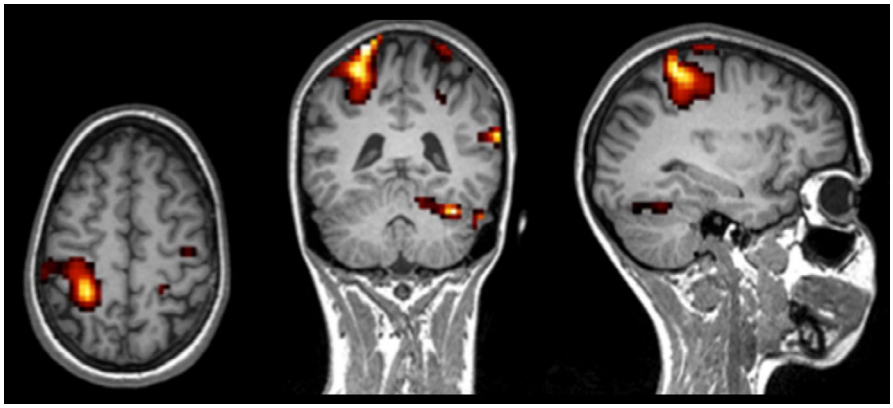

FIG. 2. BOLD activation in the right hemisphere from left hand activity. [Color figure can be viewed at wileyonlinelibrary.com]

changes during activation, comparisons are made with the resting state. Comparisons can take the form of simple subtraction, more powerful statistical methods, correlative comparisons, and generalized linear models.[131] Essentially, the active state is compared to the resting state; these are both repeated as needed during the course of the subject scan in order to build the signal to noise and time course needed to resolve the BOLD response to the activity. Note that this response is MRI signal change and is a relative measure, albeit repeatable across tasks and subjects.

The primary application of BOLD imaging is in the identification of eloquent areas critical to normal everyday activities, for example Wernicke's and Broca's areas for speech and the primary motor cortex for movement, and their relationship to areas of pathology, such as a benign or malignant masses. BOLD imaging is also known as functional MRI (fMRI). The terms are often used interchangeably as they both explicitly use magnetic resonance to detect functional activity; however, it is probably more appropriate to say that BOLD is the physiological mechanism by which brain functional activity is determined due to vascular coupling, whereas fMRI is the larger experiment by which various activation areas are targeted by providing a synchronous paradigm, typically an activity performed by the subject in the MRI.

Figure 2 shows a typical activation map obtained following an fMRI exam. Activation information, in this example resulting from left hand activity, was generated by first fitting the patient with an MRI-compatible visual and audio system that presented a synchronized stimulus or paradigm, such as a flashing checkerboard image during the activation cycle, followed by a black screen during the rest cycle. During both cycles, T_2*-weighted images were acquired and analyzed by various methods to extract the small signal change in increased activation areas. These areas can be adjusted for presentation (p, T, or Z statistic), colorized if desired, and superimposed on high resolution structural data sets (3D T_1) for treatment planning purposes. Much of the work in fMRI involves designing various paradigms, ranging from simple motor tasks, such as alternate clenching and relaxing of the hand, to more complex memory tasks, such as cuing the subject to recall picture of faces previously seen. Verbal and language paradigms help determine the topological complexity of speech and hearing/language processing.

Over the past two decades, resting state (functional) MRI (rsMRI)[132] has emerged as a task-free technique that uses advanced correlative processing to recognize coincident vascular responses in the resting brain. These correlations are also known as patterns of brain perfusion since the BOLD technique is underlying all the MRI signal intensity changes. These studies can be performed longitudinally for a given patient, or more likely, using a group analysis to determine the standard by which individuals can be compared (healthy group vs diseased individual).

fMRI(BOLD) quantification: Currently, a QIBA profile for fMRI has been written and is publicly available as an initial draft (http://qibawiki.rsna.org/images/b/b8/QIBA_fMRI_Profile_1_PC-rev1.pdf). The QIBA profile specifically and initially establishes fMRI as a biomarker when measuring the strength of the brain BOLD response from task-prescribed subject hand movements *only.* Additionally, the primary biomarker is the weighted center of mass (wCMA) of brain BOLD activation determined from the location of the BOLD foci, subject to standardized thresholding. The various QIBA assumptions must be understood and detailed activities incorporated to assure repeatability. With establishment of the biomarker, the following claim results: if the spatial location of the hand movement BOLD response can be established using a measured wCMA on a single focus, then the 95% CI for the location of the true wCMA is within 5 mm in any direction. In other words, within ± 5 mm from an initial measured center of mass ("blob" location) lie 95% of all probable activation center of mass(es). If implemented correctly, this Claim is repeatable in the same subject at different time points.

fMRI QA/QC: The QIBA fMRI profile does not describe a specific phantom for QA purposes. Instead, it recommends using commercially available head phantoms provided by either the MR scanner vendor or third party vendors. These phantoms are recommended for assessment of a range of

factors that can impact the quality of generated fMRI data including EPI ghosting in BOLD scans, interference from other equipment, gradient spiking, image distortion, overall scanner performance, fMRI stimulus delivery system and response device, fMRI SNR, and temporal SNR. To date a single, standard QA process for fMRI is yet to be established due in part to unresolved issues affecting precision and reproducibility of the fMRI data such as accurate detection of activation edges, identifying what constitutes optimal activation thresholding, the precise assessment of neurovascular uncoupling, defining acceptable limits of head motion and identifying those QC parameters that reflect BOLD activation. As a result, several approaches to fMRI QA protocols have been reported.[133,134] Although variability exists among these protocols, they do share commonalities including periodic SNR and TSNR measurements to test scanner signal and image quality, as well as operational tests of the fMRI-specific equipment (i.e., response devices, projector, goggles, audio, etc.) prior to placing the patient in the scanner.[135,136]

fMRI as a biomarker in radiation oncology: As a QIB due to the relative signal response of BOLD imaging, fMRI-derived activation areas, as shown in Fig. 2, can be considered as interval variables and qualify as biomarkers of Type 0, for example demonstrating longitudinal tumor infiltration into normally functional active areas. Additionally, functional activation areas could conceivably be used to help with treatment planning, in conjunction with tumor targeting, with a desired BOLD response as an endpoint (Type 2). This would help avoid therapy-induced damage to the normal BOLD activation regions, assuming activation is to be preserved.

Outside of the brain and as a result of the sensitivity to blood oxygen content, BOLD imaging has been investigated as a biomarker of hypoxia.[137] Given that oxygen is a known radiosensitizer, knowledge of tumor hypoxia and its spatial distribution has the potential to be a biomarker of tumor radioresistance. In this context, BOLD imaging has been combined with tissue oxygen level dependent (TOLD) imaging which relies upon T_1 signal changes as opposed to BOLD-induced T_2*to provide complimentary information of tumor hypoxia. While these two potential biomarkers are promising, it is important to note that they are in the early, preclinical stages of research and development.[138]

Biomarker strengths, weaknesses, and limitations: The local BOLD response demonstrates the potential to be a versatile biomarker as discussed above. As a biomarker of Type 0, the fMRI BOLD response departs from the classic definition of a QIB in the sense that the marker is not a representation of the natural history of a disease process. Rather, the BOLD response, as conditioned by the QIBA profile, represents the healthy function of the brain, specific to the desired stimulus, specifically to the motor cortex (hand). Thus, a healthy BOLD area may be distorted or displaced from normal by an adjacent disease process (tumor). Thus, activation areas from different activation sites (right vs left hand activation) are commonly compared when trying to therapeutically eliminate diseased tissue and safeguard functionally normal tissue.[139] Additionally, a given regional brain area, for example the motor cortex, can have significant signal differences when compared between individuals due to task compliance, native vascular organization, and analysis threshold settings. In this sense, unless a specific and repeatable set of steps is implemented, the size and color of the fMRI "blobs" superimposed on grayscale anatomy can vary significantly across subjects.

Currently, the BOLD response biomarker is limited to the motor cortex (hand) only. While there are hundreds of other brain sensory and processing areas which can be elucidated functionally via the BOLD technique, they remain to be cataloged as biomarkers in a QIBA-like fashion. Outside of the brain, there are limited applications of BOLD biomarkers. This, in addition to the narrow scope of the QIBA profile that includes only the wCMA of the activation area due to subject hand movements, means that extreme caution must be exhibited when using fMRI data in either surgical or radiation therapy treatment planning. These data should not be used as the only information to either identify irradiation volume or adjacent areas of risk, but should be used as an adjunct to established methods of target delineation.

TABLE VI. Characteristics of the MR Thermometry biomarker probe technique.

Probe technique	Temperature dependence	Biomarker type	Sensitivity	Tissue type dependent	Absolute (A) or Relative (R)
Diffusion	T	0	2% / °C	Yes	R
Proton density	1/T	0	−0.3% / °C between 37°C – 80°C	Yes	R
T_1 relaxation	T	0	~1% / °C	Yes	R
T_2 relaxation	T	0		Yes	R
Magnetization transfer	–	0		Yes	R
PRF imaging	T	0,1	−0.009 - −0.01 ppm/°C	Yes	R
PRF spectroscopy	T	0		No	A
Exogenous contrast agents	–	0		Yes	A Supplementary Material

4.B. Emergent

4.B.1. MR thermometry

Several MR tissue parameters exhibit temperature dependence that can be quantified and used as a biomarker of thermal-induced tissue (i.e., thermal therapy) damage. These temperature sensitive parameters include proton resonant frequency (PRF), diffusion, T_1 and T_2 relaxation times, magnetization transfer, proton density, and temperature sensitive contrast agents.[140,141] Table VI summarizes these biomarkers, including their temperature and tissue type dependence, sensitivity, type, and whether they quantify absolute or relative change in temperature.

Biomarker quantification: As described in Table 6, the majority of temperature biomarkers are relative, denoting a change in temperature, as opposed to absolute temperature. For these biomarkers temperature differences are quantified by application of imaging techniques that provide an MR signal proportional to the biomarker of interest. Temperature-induced signal differences are then calculated to provide an estimate of this temperature change. For example, in PRF mapping, temperature changes are quantified by the equation $\Delta T = \frac{\phi(T)-\phi(T_0)}{\gamma\alpha B_0 TE}$ where $\phi(T)$ and $\phi(T_0)$ are the phase signals at a given voxel from a gradient echo MR image obtained at the temperature of interest and a reference (baseline) temperature.[140] The parameters γ, α, B_0, and TE are gyromagnetic ratio, the PRF change coefficient, the static field strength and the echo time, respectively. In contrast, PRF spectroscopy and exogenous contrast agents provide absolute measures of temperature by comparing the frequency shift of water as a function of temperature, compared to a metabolite such as N-acetyl-aspartate or lipids that does not exhibit a temperature dependence.[140]

As QIBs, with the exception of PRF imaging, each biomarker listed in Table VI should be considered as a pre-biomarker of Type 0; PRF imaging could be considered as a biomarker of Type 1 since it is used extensively in thermal therapies, such as hyperthermia, and various ablative therapies like RF, microwave, cryogenic, and ultrasound ablation. Although a theoretical absolute zero temperature exists, these biomarkers are considered interval variables because the difference in temperature values is used for biomarker quantification. A QIBA protocol does not exist; therefore, no claims exist regarding quantifiable change in temperature known to be true within a given CI.

While PRF-based temperature measurements are most commonly used in MR-guided ablation systems, these measurements can be influenced by tissue type, susceptibility effects, electrical conductivity, motion, and magnetic field drift. Except for adipose and bony tissue, the PRF method is tissue independent. Additionally, while the magnetic susceptibility has a temperature dependence, the effect it has is small in aqueous tissues like muscle, making PRF methods robust in most clinical applications. Another potential drawback to PRF methods stems from temperature-induced changes in electrical conductivity, which may induce a phase shift, further confounding the temperature changes. Nevertheless, this effect may be of importance only when heating larger volumes, as with hyperthermia. Applications in hyperthermia may make use of mitigating methods to correct for these effects. Since PRF-based measurements rely on voxel wise changes in phase, they may suffer from motion-induced temperature artifacts. Finally, the PRF method is sensitive to the temporal stability of the magnetic flux of the magnet, which is known to drift over time; this is important to note, since many ablative treatments utilizing PRF last longer than 30 min.

Thermometry QA/QC: Currently, no formal QA procedures exist for MR-derived estimates of absolute or relative change in temperature. Gorny et al[142] reported on acceptable testing procedures for MR-guided focused ultrasound therapy systems that include the use of PRF-derived temperature estimates to characterize the performance of the ultrasound system, but they did not provide specific recommendations of assessment of accuracy of temperature measurements. The AAPM Task Group 241 on MR-guided ultrasound is expected to formally publish recommendations on intrinsic system characteristics, quantitative metrics, and quality assurance measures.[143] Until formal QA procedures are published, individual sites using MR thermometry techniques are encouraged to establish their own protocols.

MR thermometry in radiation therapy: To date, the application of MR thermometry in RO is limited. Currently, MR thermometry for hyperthermia (i.e., increasing tissue temperatures ranging from 40°C to 42°C for 30–60 min) is a growing area of clinical research in oncology due to its role in radiosensitization and chemosensitization.[144] With the development and clinical translation of MR linear accelerators (i.e., MR-linacs), it is foreseeable that a future application of temperature mapping will be developed but will require the establishment of appropriate QA protocols and related assessment of accuracy and precision of these measurements.

MR thermometry derived temperature's primary role as a biomarker is to quantify and monitor thermal injury. Tissue ablation using heat is measured in terms of the thermal dose, t_{43} where $t_{43} = \int_{t=0}^{t=final} R^{\frac{43^oC - T(t)}{1^oC}} dt$, R is the number of minutes needed to compensate for 1°C temperature change above or below 43°C, and T(t) is the temperature at time t which is equal to the time required to produce the resultant effect at a temperature of 43°C.[145] Ultrasound induced tissue ablation is considered to have occurred in both normal (i.e., normal tissue toxicity) and disease (ablation) when t_{43} is equal to 240 min.[145]

Biomarker strengths, weaknesses, and limitations: MR thermometry methods have been implemented in a number of in vivo applications, providing information about the response to thermal tissue ablation in real time. Temperature

measurements during motion or in the presence of adipose or fatty tissue remain challenges for this technology. Absolute temperature measurements, especially with excellent spatial and temporal resolution, are challenges, as well. Nevertheless MR thermometry using the PRF method seems to be the most sensitive and widely used method for monitoring thermal therapies. The usefulness of any method, although, varies dependent on tissue type, application, anatomy targeted, and magnetic field strength, making comparisons between methods quite challenging.

4.B.2. Chemical exchange saturation transfer (CEST)

CEST generates a contrast in MR images based on chemical exchange of free water protons and protons of solute molecules. From the many exogenous and endogenous molecules introduced as CEST contrast agents, CEST contrast mediated by Amide Proton exchange in tumors such as gliomas may have direct application for diagnosis and in response assessment. Amide Proton Transfer weighted imaging (APTw) is a contrast free CEST imaging technique utilizing endogenous cellular proteins to produce an MR signal that directly correlates with cellular proliferation.[146-148]

CEST imaging involves the application of a frequency selective saturating RF pulse to label amide groups in proteins/peptides. Due to chemical shifts, the resonant frequency of the labeled protons will be different from bulk water (i.e., they are off-resonance). The peptide signal amplifies by 100–1000 times through the process of chemical exchange with water, governed by the chemical exchange rate constant (k) while the bulk water signal decreases. The magnitude of the subsequent reduction of bulk water signal consequently depends on the dynamics of chemical exchange, as well as the ratio of exchangeable solute protons to bulk water protons. The rate constant of chemical exchange itself is influenced by the pH value and the temperature within the exchange environment. If the latter two parameters can be assumed to be distributed homogeneously in tissue, the CEST effect can be a surrogate marker for the concentration of a certain species of solute molecule in the tissue.

In order for a solute molecule to be considered suitable as an endogenous CEST agent, it must carry labile protons that exchange with bulk water at exchange rates that fulfil the condition $k \leq \Delta\omega$, where $\Delta\omega$ is the resonance offset of the solute protons to the water protons measured in s^{-1}. The most common method for acquisition of a CEST data set is to acquire multiple image data sets with presaturation at different offset frequencies (S_{Sat}) around the water resonance, and one reference data set without saturation (S_0) or with saturation at a very large offset frequency.[146] The normalized signal as a function of the presaturation offset (z-spectrum) can then be used to determine and quantify CEST effects, which are asymmetric with respect to the water resonance (i.e., a CEST effect appears either up- or down-field from water and can hence be extracted from the z-spectrum via analysis of its asymmetry with respect to the water resonance). The measure of a CEST effect obtained through such an asymmetry analysis is regularly referred to as MTR_{asym}, which is always expressed as the relative change in bulk water signal. Nevertheless, in vivo z-spectra are inherently asymmetric because of conventional magnetization transfer (MT) effects. Additionally, CEST effects are masked by concomitant direct water saturation as a result of the bandwidth of the saturation pulses.

Figure 3 illustrates the use of anatomic and CEST imaging in a patient diagnosed with a glioma tumor. Image comparison demonstrates that ATPw provides additional details of the metabolically active tumor core and region of tumor invasion not revealed by anatomic imaging alone. CEST imaging may therefore uncover areas for targeting, such as dose painting, as well as identifying areas of treatment failure.

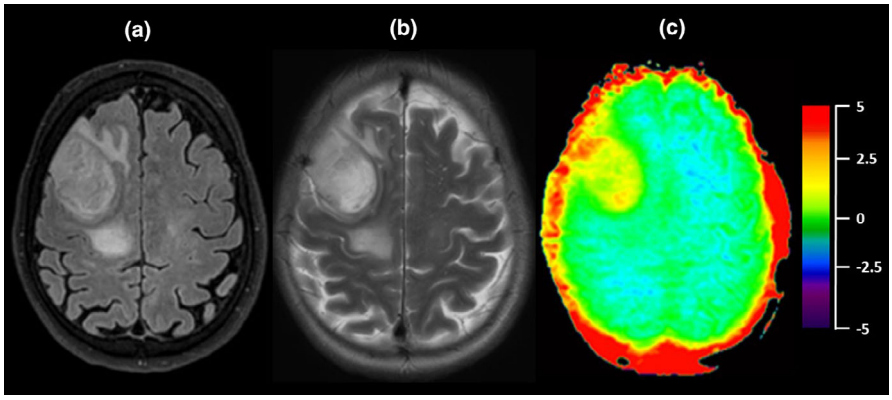

FIG. 3. Anatomic and CEST image data patient with a glioma acquired at a field strength of 3T. (a) T_2-weighted image (TE/TR/fa/Scan duration = 117 ms/4000 ms/90°/1 min:28 s, voxel dimension = 0.6 mm × 0.6 mm × 5 mm). (b) T_1-weighted FLAIR (TE/TR/fa/Scan duration = 316 ms/480 ms/90°/5 min:41 s, voxel dimension = 1.1 mm × 1.1 mm × 1.2 mm). (c) CEST APTw image (TE/TR/fa/Scan duration = 8 min:18 s/5928 ms/90°/3 min:45 s, voxel dimension = 1.78 mm × 1.8 mm × 6 mm). Anatomic data (a-b) show an iso- to hyperintense mass lesion in the frontoparietal region. The APTw weighted image (c) indicates a metabolically heterogeneous tumor with an active core and pretumoral spread along the anterior lateral rim of the mass. TE = echo time, TR = repetition time, fa = flip angle, FLAIR = fluid-attenuated inversion recovery. Data courtesy of Krankenhaus der Barmherzigen Brüder (Trier, Germany) and Philips Healthcare (Best, Netherlands). [Color figure can be viewed at wileyonlinelibrary.com]

CEST/APTw quantification: CEST imaging provides spatial information on the relative distribution of specific metabolites relative to water.[148] As such, CEST images are typically presented as percentage maps. A quantitative biomarker, CEST information can be considered as an interval variable in which the differences between percentage metabolite concentrations within an image provide information on disease stage and extent. As a QIB, CEST values can be considered as a Type 0 biomarker in which the values derived from these images are considered interval variables due to the relative nature of their values.

CEST/APTw QA/QC: CEST imaging and APTw are emerging techniques. QIBA does not describe a specific phantom or protocol for QA purposes. Nevertheless, QA phantoms and methods will be needed as endogenous and exogenous molecules become available for CEST imaging.

CEST/APTw in radiation oncology: CEST imaging has the potential to be a valuable biomarker in RT for diagnosis by identification of specific metabolites within a tumor, and for measurement of therapeutic response; however, current literature is relatively sparse to establish the sensitivity and specificity of these data. Ongoing research and clinical evaluation demonstrating a high clinical level of evidence are therefore needed to fully characterize this biomarker.

Biomarker strengths, weaknesses, and limitations: CEST imaging has been employed in a number of clinical imaging research centers worldwide, producing semiquantitative results. While endogenous biomolecules with amide have been detected and are promising for solid tumor assessment, the level of clinical evidence and degree of technical efficacy means that this biomarker is considered as a Type 0. That is, CEST has been demonstrated to correlate with extracellular pH which is known to be altered in malignancy[149,150] and while studies have also demonstrated correlation with cancer aggressiveness and treatment efficacy,[151,152] these data are single center preliminary reports that require extensive ongoing validation. As a QIB CEST derived values are classified as interval variables.[147] In general CEST pulse sequences demand long duration saturation pulses, with acquisition at multiple saturation frequencies, and with long repetition times to allow for relaxation, all of which result in long scan times. The APT technique itself is sensitive to motion. Additionally, static magnetic field and RF field in homogeneities present a challenge for the CEST technique, which, when measuring the CEST effect, must take these into account and be optimized. Nevertheless, endogenous CEST applications, such as APTw imaging show great potential as an emergent MR biomarker.

4.B.3. Hyperpolarization (HP)

While ^{1}H MRI and MRS techniques provide valuable insights into anatomical and physiological changes associated with cancer, several other molecules have the potential to elucidate additional information but they have been used sparingly due to their low concentrations in vivo. To address this deficiency, several methods have been developed to increase the net magnetic polarization of the nucleus under investigation through a process referred to as HP.[153] Depending upon the nucleus and method, polarization levels of almost 100% compared to the native values, which can be of the order of 1/10000th of a percent, can be achieved, thereby increasing the SNR of the nucleus of interest to detectable levels. Thus, HP techniques address the relatively limited abundance of the molecular species of interest, as well as the lower gyromagnetic ratio, compared to ^{1}H, and in doing so create opportunities to study biologically important compounds and processes that could not be obtained otherwise.

HP ^{13}C Magnetic resonance spectroscopic imaging: HP ^{13}C is one of the most promising nuclei and has potential to further improve the clinical assessment of cancer, in particular, by providing an improved assessment of disease type, stage, and aggressiveness, and for monitoring treatment response.[154] While clinical ^{13}C spectroscopy has historically been limited by its low natural abundance of ^{13}C (1.1%) and gyromagnetic ratio (γ of ^{13}C is one quarter that of ^{1}H), this has been overcome two ways: (i) by the ^{13}C labeling of important metabolic substrates such as [1-^{13}C]pyruvate, in which the C-1 position is synthetically labeled with close to 100% ^{13}C nuclei, and (ii) by prepolarizing these substrates using dynamic nuclear polarization (DNP) before injection into either preclinical cancer models or patients with cancer.[153,154] The unprecedented gains in sensitivity (>10,000-fold signal increase) provided by DNP has allowed the in vivo acquisition of both single time point high spatial resolution ^{13}C-MRSI and time-resolved metabolic kinetics that reflect flux through enzyme-catalyzed reactions previously inaccessible by ^{1}H spectroscopy.[154,155]

The detection of flux through individual enzyme-catalyzed reactions offers a fundamentally new approach to imaging and understanding disease biology, and this approach is clinically translatable.[156,157] The most promising HP substrate to date is [1-^{13}C]pyruvate, which provides the following: monitoring of a key metabolic pathway, conversion of [1-^{13}C]pyruvate to [1-^{13}C]lactate (k_{PL}) via the enzyme lactate dehydrogenase (LDH), which is highly upregulated in most cancer types (the "Warburg effect"); high levels of polarization via dissolution DNP; and biocompatibility at doses of 0.43 ml/kg body weight and 250 mM, as determined in a phase 1 safety trial.[157,158] In addition, published studies have demonstrated a mechanistic link between increased HP lactate signal and other cancer-associated cellular alterations, such as the elevated expression of lactate dehydrogenase A (LDHA) and monocarboxylate transporters (MCTs), and lowered pH in the extracellular environment. The accompanying reduction in PDH (pyruvate dehydrogenase) activity can also be directly measured via levels of pyruvate C_1-derived bicarbonate and [5-^{13}C]glutamate from [2-^{13}C]pyruvate.[159]

HP ^{13}C MRSI encodes chemical and spatial information, thereby providing the potential for using multiple HP ^{13}C labeled MR probes to detect several metabolic and/or physiologic processes simultaneously after the injection of a single bolus.[160] A number of ^{13}C labeled bio-molecules other than pyruvate have been suitably hyperpolarized; preclinical studies have shown the potential for several of these ^{13}C labeled probes to provide information about metabolism ([5-^{13}C]glutamine), perfusion (^{13}C urea), pH (^{13}C bicarbonate), and cellular redox status ([1-^{13}C]dehydroascorbate).[154] Additionally, HP ^{13}C MRSI can be performed on a standard clinical MRI scanner that has been enabled to acquire ^{13}C data, allowing it to be added to clinical ^{1}H MRI exams.

Biomarker quantification: Absolute quantification of the HP pyruvate and its metabolites is difficult owing to several factors, including differences in polarization and simultaneous signal loss due to T_1, metabolic conversion and RF sampling. For this reason, ratiometric analyses of pyruvate and lactate signal intensities have been the simplest and most commonly used method to distinguish normal from diseased tissues and following therapy. Dynamic imaging acquisition in HP ^{13}C MRI offers the potential to provide robust quantification of metabolic conversion, regardless of differences in bolus delivery.[161] This is in contrast to imaging at a single time point which can be analyzed via the lactate-to-pyruvate ratio,[162] but is very dependent on experimental timing. Dynamic imaging acquisitions can be analyzed using kinetic modeling, typically to calculate a pyruvate-to-lactate metabolic conversion rate, k_{PL}.[158]

Pyruvate is converted into lactate by LDH and cofactor nicotinamide adenine dinucleotide + Hydrogen (NADH) via an ordered ternary complex. The velocity of the reaction (V_{eq}, in Mol/s) as a function of reagent concentrations can be derived using classical enzyme kinetics.[163] Despite the underlying complexity, at present and under the assumption of physiologically relevant conditions, this reaction in vivo is typically summarized using a first-order two-site exchange model[164-168] utilizing a single apparent chemical conversion rate constant (k_{PL}, with units s^{-1}). Chemical interconversion of HP pyruvate and lactate in vivo is described by $k_{PL} = V_{eq}/(P + P^*)$, where P and P^* represent the concentration of unlabeled and enriched HP "visible" pyruvate pools, respectively.[169] Another popular approach is to use the AUC ratio from dynamic lactate and pyruvate data, that under assumptions of constant-in-time flip angles acquired prior to bolus arrival or consistent bolus characteristics, is directly proportional to k_{PL}.[167] Therefore, kinetic analysis of the spatial and chemical endpoints of HP pyruvate can provide a quantitative minimally invasive imaging biomarker for changes in metabolism with malignant transformation and in response to therapy.

As a biomarker, HP ^{13}C can be considered as Type 0 due to its early phase of technical development and clinical assessment. More specifically, while the underlying biological mechanisms of action are known, significant work remains including the need for preclinical and multicenter clinical trials as well as regulatory approval which are needed to transition HP ^{13}C to a Type 1 and eventually Type 2.[170] In addition it can be considered a ratio variable, as there is the potential for a true zero value of the concentration of HP ^{13}C. It is expected that this biomarker will quickly transition from Type 0 to Type 1.

HP ^{13}C MR QA/QC: Due to the early stages of development and clinical translation of HP ^{13}C MRSI, a QIBA profile or standardized QC/QA program and phantom does not exist. To this end, preclinical studies and early patient validation studies have established that a dynamic HP ^{13}C MRI imaging approach is required in order to deal with differences in the delivery of HP ^{13}C probes.[157,158] Additionally, an enzyme-based phantom system providing reproducible dynamic chemical conversion of HP pyruvate into lactate was designed and implemented to validate the performance of MR scanner hardware and acquisition as well as data modeling strategies. This phantom was also used in the first multicenter trial of hyperpolarized [1-^{13}C]pyruvate entitled "Multi-Site Development & Evaluation of a Quantitative 3D Hyperpolarized ^{13}C MRI Clinical Prostate Cancer Exam."[169,171]

HP ^{13}C MR as a biomarker in radiation oncology: HP ^{13}C pyruvate MRI has been used successfully in several preclinical and clinical studies to monitor response to treatment via a range of anticancer therapies, including DNA-damaging agents, radiotherapy, antivascular agents, targeted therapies, hormonal therapy, and antimetabolites. All of these have been reported to lead to a drop in HP lactate labeling, mediated by different mechanisms in the various treatments.[153-155] These data have been instrumental in linking measurements obtained from HP MRI imaging of pyruvate to post-therapy cancer viability and aggressiveness. Specifically, in animal models, the conversion of HP pyruvate into lactate is reduced in tumors following exposure to ionizing radiation (XRT). A reduction in HP lactate has been observed in murine models of glioma 72 h after 5 Gray of radiation,[172] MDA-MB-231 breast adenocarcinoma 96 h after 16 Gray of radiation,[173] and SCCVII squamous cell carcinoma and HT-29 colon cancer 1 day after conclusion of fractionated (3 × 10 Gray) XRT.[173-175]

A phase 1 clinical trial in prostate cancer patients demonstrating the safety and imaging feasibility of HP [1-^{13}C]pyruvate MRSI has been completed,[157] and there are a number of ongoing clinical trials at several institutions involving patients with prostate cancer, breast cancer, brain tumors, liver metastases, and heart failure.[156,176-178] In the case of prostate cancer, early patient validation studies involving test–retest reproducibility, correlations with pathologic findings, and clinical outcomes such as survival and disease progression after treatment have been initiated. In advanced prostate cancer, 6 weeks after effective androgen deprivation- and chemo- therapy, a

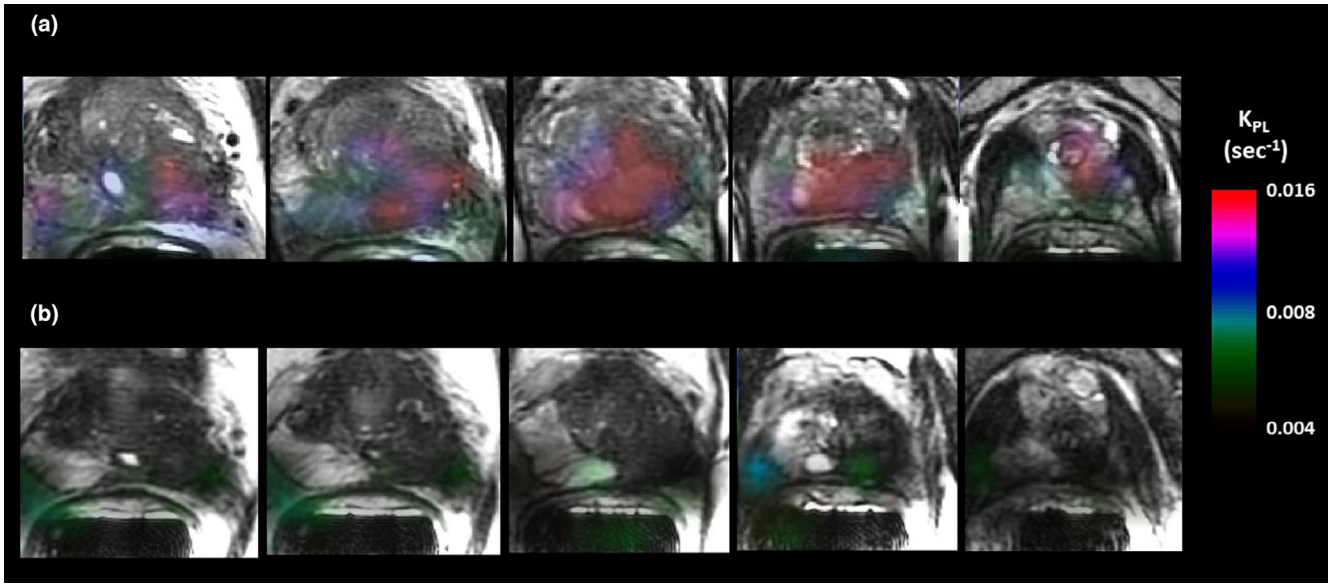

FIG. 4. Contiguous axial T_2-weighted anatomic images with overlaid pyruvate-to-lactate metabolic conversion rate(k_{PL}) images (base to apex) of a 52-year-old patient with extensive high grade prostate cancer prior to therapy. (a) Pretreatment regions of high k_{PL} were consistent with biopsy proven Gleason score 4 + 5 and 4 + 4 cancer throughout the left lobe and Gleason score 4 + 3 in the right midgland. (b) Six weeks postandrogen deprivation- and chemo-therapy, multiparametric ^{1}H MRI indicated the presence of residual cancer; in contrast, k_{PL} was dramatically reduced (k_{PL} max pre ~.025, post ~ 0.007 sec^{-1}), consistent with a significant reduction in serum prostate specific antigen (25.7–0.78 ng/ml). [Color figure can be viewed at wileyonlinelibrary.com]

significant early reduction in k_{PL} preceded changes in mp-^{1}H MRI and predicted clinical response (Fig. 4).[156,176-178]

Following promising preclinical studies in brain tumors, multiple sclerosis, and traumatic brain injury, the feasibility of using HP ^{13}C MRI for evaluating brain metabolism in patient studies was recently established.[177,178] These studies demonstrated that [1-^{13}C]pyruvate is transported across the blood–brain barrier, and that conversion to [1-^{13}C]lactate can be detected in regions of tumor and normal brain. Interestingly, the rate of conversion in normal brain was substantially higher than had previously been observed in anesthetized preclinical models. For dynamic slab-localized and 2D echo planar spectroscopic imaging data with 4–8 cc spatial resolution, it was also possible to observe the conversion of HP pyruvate to bicarbonate, which may discriminate between tumor and normal brain. Single institution studies with NIH funding include protocols for obtaining data in primary brain tumors prior to image-guided surgery, and for comparing that conversion to [1-^{13}C]lactate/[1-^{13}C]pyruvate in patients pre- and post-treatment with radiation and temozolomide.

Biomarker strengths, weaknesses, and limitations: As a biomarker in RO, HP ^{13}C MRSI could prove useful in evaluating prognosis and indicating overall response akin to the use of FDG PET/CT in lymphoma.[179] In this context, the role of HP would be to determine whether or not treatment has eliminated the malignancy, as well as to help determine if there is a need for additional treatment by predicting the likelihood of disease relapse or progression.

Although HP ^{13}C has significant promise to provide new and quantitative insights for RO, several limitations and weaknesses remain. The short half-life of HP ^{13}C (65−70 s for [1-^{13}C]pyruvtae at 3T) necessitates the need for onsite DNP polarizer (SPINlab, GE Healthcare) and related preparation and handling spaces similar to what is needed for short half-life ^{11}C PET probe production. An onsite hyperpolarizer represents a financial investment and requires associated technical and professional staff required to run and maintain the unit, limiting the dissemination of this technology to the broader RO community. The success of the phase 1 clinical trial resulted in the rapid proliferation and clinical research use of commercial SPINLab polarizers. Despite the expense, more than 20 sites currently have SPINlab polarizers, seven have performed HP [1-^{13}C]pyruvate human studies (resulting in 200+ patient studies in brain, heart, prostate, and liver thus far), and 5+ sites are in the final planning stages. Another limitation of HP ^{13}C is the need for ongoing validation and quantification in order for it to become a true QIB. Analytic validity will be an important question, as clinicians need to understand what HP ^{13}C MRSI is measuring and see evidence that these measurements are accurate. Demonstrating the reproducibility of hyperpolarized imaging exams is another important step, requiring established standards and repeatable methods for HP ^{13}C MRSI data acquisition and interpretation. Clinical validity remains to be established, as well. HP ^{13}C MRI results must be compared to an accepted clinical standard such as the tissue or laboratory-based assays. In assessing the clinical utility, clinicians will look for validation against clinical outcomes, accuracy (sensitivity, specificity, ROC area) vs a reference standard in diagnostic applications, and predictive accuracy in assessing therapeutic response, as described previously for other considered biomarkers.

4.B.4. Magnetic resonance elastography (MRE)

MRE is a phase-contrast based method of quantifying the mechanical properties of biological and biologic-like materials. The technique, first described by Muthupillai et al,[180] involves the visualization of cyclic displacements induced by propagating acoustic (i.e., shear) waves within the object under interrogation and encoded in the phase of the MR signal. Synchronization of the external motion source and motion sensitizing gradients allows sampling of the shear wave at predetermined phase offsets of the shear wave cycle. This information is then processed by a mathematical operation known as inversion,[181] in which an estimate of the shear modulus of the material is obtained. Since the inversion operation is performed at each pixel, the output is a quantitative topographical distribution of the intrinsic mechanical properties of the material under interrogation and is commonly referred to as an elastogram.

A variety of both benign and malignant disease processes alter the intrinsic mechanical properties of tissues,[182] a phenomenon that is utilized by one of the oldest and most cost effective methods of the physical exam, palpation. For solid malignant masses, their mechanical properties are known to increase due to a variety of factors, including the generation of compressive and tensile forces due to tumor growth, increasing stiffness of density of the extracelluar matrix (ECM), and an increase in interstitial fluid pressure due to angiogenesis and breakdown of the endothelial barrier.[183] In contrast, at the cellular level, malignant cells are known to be softer than their nonmalignant equivalents,[184] pointing to the significant contribution to overall tumor stiffness by the ECM and its constituents.[182] Increased ECM stiffness plays an additional, important role in the promotion of tumorogenesis and metastatic potential[183] by means of mechanotransduction,[185] the process of conversion of mechanical forces into chemical signals, effectively creating a feedforward mechanism in which increasing stiffness of the ECM promotes both the growth of malignant cells and related growth factors.[184] In nonmalignant fibrotic diseases tissue stiffness is also known to increase due to remodeling of the ECM, primarily through the increased deposition of collagen.[182] Malignant and fibrotic diseases share many common characteristics: increased overall stiffness, remodeling of the ECM, and a feedforward process whose primary mode of action is increased stiffness. In fact, malignant tumor growth has been described as the "wound that does not heal".[186]

In a perfectly elastic material in which there are no viscous losses, the shear modulus (μ, the ratio of shear stress to shear strain) of the material is related to the shear wave speed (V_s) by the equation $\mu = \rho V_s^2$ or $\mu = \rho (f\lambda_{sp})^2$ where ρ is the density of the material, f the frequency of the mechanical excitation, and λ_{sp} the spatial wavelength of the propagating shear wave. Early MRE inversion algorithms assumed that tissue was perfectly elastic, estimating μ by spatially resolving λ_{sp} and assuming that tissue density was equal to 1.0 g/cm^3 (i.e., unity). To reflect the fact that these algorithms ignored the effects of viscosity, the quantitative values generated have been referred to as estimates of shear stiffness as opposed to shear modulus. Recent advances in MRE inversion algorithms have included the effects of viscoelasticity, thereby providing a more accurate estimate of the true elastic properties of human tissues and organs.[187] Inclusion of viscoelastic effects provides a complex estimate of shear modulus G* in which both the storage (G') or elastic and loss (G'') or viscous components are calculated.[181,188] Within the context of this work, stiffness refers to the general mechanical properties of tissue, shear stiffness to elastograms generated by MRE inversion methods that assume a perfectly elastic medium, and shear modulus those techniques that include viscous losses. In all circumstances, MRE elastograms are quantitative, providing estimates of the intrinsic shear mechanical properties of the material under investigation in kilopascals (kPa).

MRE quantification: MRE derived estimates of G* of tissue can be considered as a QIB of Type 0, while actual stiffness values are considered ratio variables. At the time of publication, a MRE QIBA profile has been published and is considered a consensus profile (http://qibawiki.rsna.org/images/f/f6/MRE-QIBA_Profile-2019-06-06-CONSENSUS-maintenance.pdf). The relatively nascent nature of this biomarker is reflected in the fact that the profile only pertains to liver fibrosis and implicitly excludes other organs and disease processes known to increase liver stiffness. The profile provides the claim that a change in hepatic stiffness of 19% or larger represents a true change in stiffness with a 95% confidence interval (CI) measured over two time points on the same scanner, MRE driver hardware, acquisition parameters and software.

MRE QA/QC: The MRE QIBA profile provides recommendations for MRE QA which includes compliance with MR scanner manufacturer and accreditation body general QA programs. In addition, the profile describes an optional QA program to ensure the proper functioning of the MRE system that involves scanning a cylinder of dimensions 12.5 cm × 15.5 cm (diameter) of wall thickness of 0.15 cm filled with polyvinyl chloride (PVC) typically supplied by the MR equipment vendor. A bi-annual testing frequency is recommended in which differences in average stiffness between measurements of ≤10% are considered within acceptable limits. It is important to note that at the time of this report, a standardized universal MRE QA phantom and testing protocol does not exist.

MRE as a biomarker in radiation oncology: The most widely used clinical application of MRE is for the diagnosis of liver fibrosis[189]; as such, the application of MRE in the diagnosis of cancer, as well as the response to therapy (chemotherapy and/or radiation therapy), remains largely unexplored. Figure 5 demonstrates MR elastograms derived from two patients: one with a benign cavernous hemangioma located in the left lobe of the liver, the other with a malignant

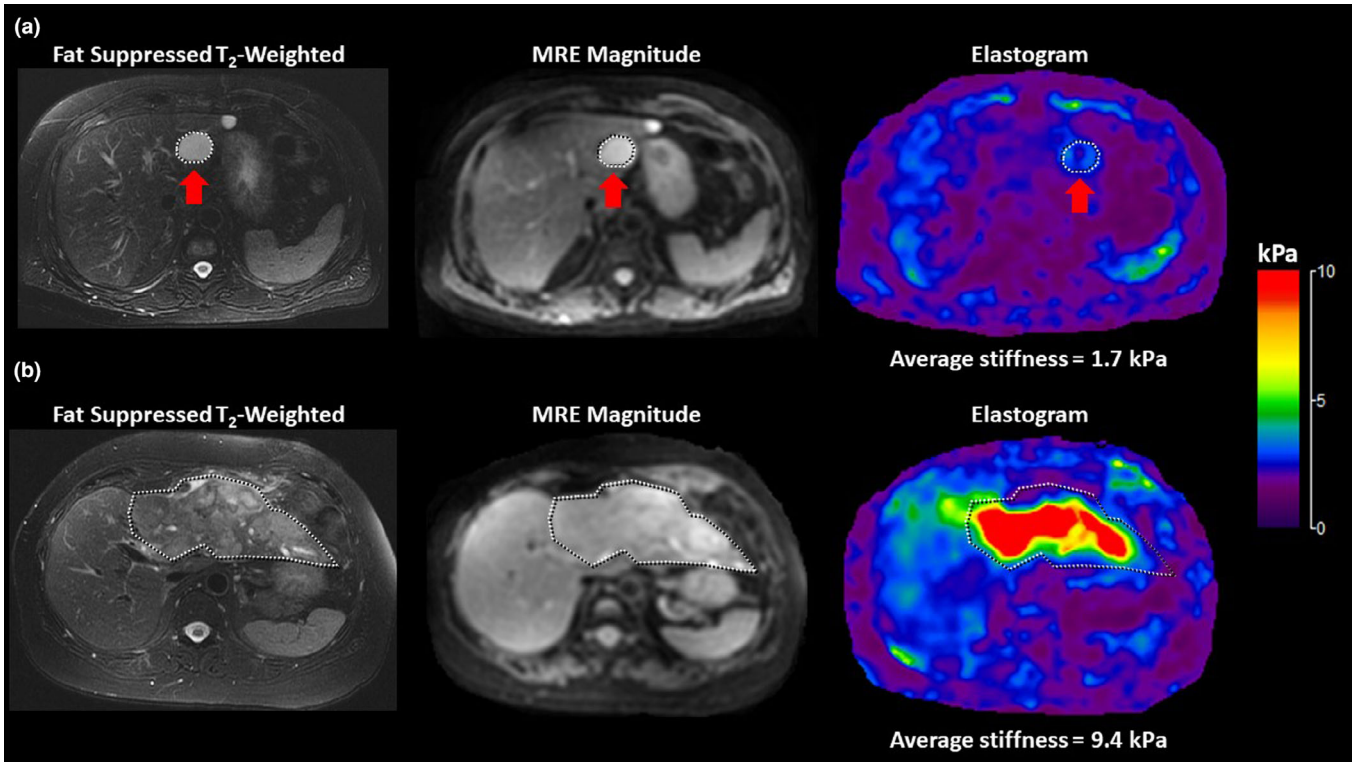

FIG. 5. Fat saturated T_2-weighted, MRE magnitude and elastogram images of benign and malignant masses in the liver. (a) Benign cavernous hemangioma (red arrow) located in the left lobe of the liver with an average stiffness of 1.7 kPa. (b) Malignant cholangiocarcinoma (outlined) located in the left lobe of the liver with an average stiffness of 9.4 kPa. [Color figure can be viewed at wileyonlinelibrary.com]

cholangiocarcinoma in the left lobe of the liver. The malignant mass is over five times stiffer than the benign mass. Preliminary results from Pepin et al[190] demonstrated that MRE-derived tumor stiffness is altered in non-Hodgkin's lymphoma following administration of chemotherapy and that these changes precede volumetric changes. In addition, differences in MRE-derived stiffness between normal and malignant tissues have been quantified by numerous groups in a variety of organs and cancer types including the breast, prostate, brain, and liver. In general, solid malignant tumors are harder (i.e., stiffer) than benign or nonmalignant tissue within the same organ.[191] Stiffness profiles of brain tumors are considerably more heterogeneous with both benign and malignant tumors exhibiting stiffness values ranging from less than (i.e., softer) to larger than (i.e., harder) normal brain parenchyma.[192] Recent research[193] indicated that glioma grade is inversely related to shear stiffness, and that differences in stiffness are associated with mutation of the IDH1 gene.

Biomarker strengths, weaknesses, and limitations: MRE is a potentially powerful oncologic biomarker providing additional diagnostic information (i.e., tissue stiffness) noninvasively. It quantifies the spatial topography of tissue stiffness, thereby identifying areas of higher/lower grade disease within a given mass, and has the potential to provide information on treatment response significantly earlier than conventional imaging-based criteria such as RECIST. Ongoing research also indicates that MRE can also provide a range of stiffness-related biomarkers, such as the storage and loss modulus as well as the damping ratio. As an emergent biomarker it is apparent that the full utility of MRE is yet to be realized, particularly in oncology-related indications and applications.

Several limitations and challenges exist related to the use of MRE-derived estimates of tissue stiffness. Because of the emergent nature of this biomarker, there are limited data on tissue and organ stiffness for normal and disease conditions. As a biomarker in RO, there is less data, particularly in determining response to therapy and normal tissue toxicity. Additionally, there is a lack of standardization of acquisition techniques, mathematical processing algorithms, and QA/QC, with the exception of liver MRE for which a QIBA profile exists. With the development of 3D MRE techniques, spatially accurate shear wave displacement fields can be sampled, allowing more precise estimates of tissue stiffness and providing the opportunity to assess focal disease; however, there remains a spatial resolution limit beyond which stiffness estimates are no longer considered reliable. It is important to appreciate that there is no single spatial resolution value (e.g., a given pixel size in mm) for which MRE stiffness estimates can be considered valid or invalid. This is because this limit is dependent upon multiple factors, such as driving frequency, geometry, and other acquisition parameters which are unique to a given MRE application, disease process, and organ. As such, MRE-derived estimates of tissue stiffness (i.e., G^*) cannot be used to direct RT treatments, either

directly by means of importation into RT treatment planning systems, or indirectly through visual inspection of elastogram data sets.

4.B.5. Fat quantification

Body fat content can be assessed using both imaging and spectroscopic techniques that rely upon a shift in the resonant frequency of protons in fat compared to water.[194] The shift, known as the chemical shift effect, is equal to approximately 3.5 parts per million of the resonant frequency of water. Because resonant frequency is field strength dependent, the shift is equal to 220 Hz at 1.5 T and 440 Hz at 3.0 T, with lipid-bound hydrogen having a lower resonant frequency compared to water.[194] While chemical shifts between water and fat signals can produce so-called chemical shift artifacts of the first and second kind, these effects form the basis of both spectroscopic and fat imaging techniques.

Spectroscopic assessment of fat content involves assessment of the spectrum of resonant frequencies of protons within a given voxel of tissue. The two most common approaches are known as point resolved spectroscopy (PRESS) and stimulated echo acquisition mode (STEAM).[195] In reality, fat consists of several types of hydrocarbon combinations (CH, CH_2, CH_3), and spectroscopy provides a method to both quantify and differentiate individual chemical species. PRESS and STEAM approaches, although, are dependent upon pulse sequence parameters, with PRESS providing an overestimate of fat content when compared to STEAM.[195] Independent of technique, the fidelity of the spectroscopic data is highly dependent upon the homogeneity of the B_0 field. As such, B_0 shimming techniques are essential, as well as imaging of tissue which is relatively homogeneous. Spectroscopy is also highly sensitive to the effects of motion.

All imaging-based approaches rely upon the chemical shift between fat and water protons but vary in their accuracy and complexity. The simplest approach is to perform suppression of the fat signal using RF pulses tuned to the resonant frequency of fat. Acquisition of a second image without suppression of the fat signal provides a fat and water image. Subtraction of the two data sets provides an estimate of the fat only content. While straightforward and implementable on all commercial MR scanners, this approach is the least quantitative.[194] Like the chemical saturation approach, so-called dual echo Dixon methods obtain two image data sets in which the fat and water signals are either in phase or 180° out of phase. It can be easily shown that subtraction and addition of the two data sets provides an image of the fat only and water only content.[194] Like chemical saturation methods, dual echo Dixon techniques are prone to B_0 inhomogeneities and can produce errors in the estimation of fat content, the most common of which is the so-called fat-water signal swap. The most robust approach to fat quantification is the use of multiecho (typically 3 or six)[196] iterative reconstruction methods in which the fat and water signals are out of phase at phase angles that are no longer integer increments of 180°.[197] These algorithms provide a method of estimating and therefore correcting for B_0 inhomogeneities. Thus, they are less susceptible to fat-water swaps and other artifacts.

Quantification: Within the MR imaging community, consensus is developing regarding the most accurate and practical approach to fat quantification, known as the proton density fat fraction (PDFF).[198] The PDFF is simply the ratio of the fat to fat + water signal ($PDFF = \frac{S_F}{S_w+S_F}$ where S_w and S_F are the water and fat signals, respectively), in which confounding factors such as T_2*, T_1 spectral shifts, and noise bias are corrected.[199] As such, the PDFF can be considered as a ratio variable, given that a value of zero is likely improbable. As a QIB the PDFF can be considered as a Type 0, given that body fat content is a known contributor to a variety disease states with PDFF values being ratio variables.

Fat quantification QA/QC: While PDFF is being recognized as the most precise and reliable biomarker for quantitative assessment of body fat content, standardized QA/QC programs do not exist. To address this limitation, a QIBA FDFF Biomarker committee has been established (http://qibawiki.rsna.org/index.php/PDFF_Biomarker_Ctte), however, at the time of writing, a PDFF profile is not available. It is expected that the finalized protocol will contain standardized profile components, including standardized imaging protocols, QA/QC programs, and phantoms.

Fat quantification as a biomarker in radiation oncology: Initial interest in quantification of fat content stems from the role of body fat content (i.e., obesity) in disease stage and progression, as well as overall health in general. More recently, interest in quantification of PDFF has increased due to the recognition that nonalcoholic fatty liver disease (NAFLD) is the most common liver disease in the United States, and that hepatic steatosis is a primary feature and the earliest manifestation of this disease.[200]

While the role of PDFF in oncology is yet to be established, initial studies suggest that this biomarker is diagnostic and prognostic and provides insight into therapeutic response. Van Gemert et al[201] identified that loss of body fat in postmenopausal women was associated with changes in a variety of biomarkers that are known to be associated with increased risk of breast cancer. A literature review extending over 20 yr by White et al[202] identified a similar association between increased risk of hepatocellular carcinoma with NAFLD and with nonalcoholic steatohepatitis (NASH, i.e., fatty liver). As a biomarker of therapeutic response, changes in bone marrow fat content in patients undergoing radiation and chemotherapy have been described,[203,204] along with a dose response relationship between fat content and radiation and chemotherapy.[204] Visceral fat area has been identified as being predictive of outcome in both colorectal[205] and metastatic renal cell carcinoma[206] treated with targeted antiangiogenic chemotherapy agents, supporting the fact that adipose

tissue releases angiogenic factors known to promote tumor growth. While these findings are encouraging, it is important to note that, as with other emergent biomarkers, extreme caution should be exhibited when using PDFF values in treatment planning and treatment response decisions.

Biomarker strengths, weaknesses, and limitations: As mentioned, T_1 and $R_2^*(1/T_2^*)$ weighting are the primary contrast confounders to PDFF. R_2^* shortening caused by iron is the most common factor impacting accuracy in hepatic measurements, as rapid signal decay can severely impact the signal of the second gradient echo in a phase sensitive experiment. Fat and water signals are modeled by a simple two-peak spectroscopic model, even though fat is known to have several spectral peaks (5.3, 4.3, 2.1, 1.3, and 0.9 ppm), whose relative contributions could vary by fat type and anatomical site. However, the two-peak spectroscopic model has the minimum number of parameters to fit, and thus is most robust and most broadly implemented. Overall, PDFF is believed to have excellent repeatability and reproducibility. A meta-analyses published by the RSNA-QIBA PDFF Biomarker Committee found excellent repeatability and reproducibility in 11 studies, with a standard deviation of only 1.08% absolute PDFF value under repeatability conditions and a standard deviation of 1.48% absolute PDFF value under reproducibility conditions when measurements are made within the same ROI. Reproducibility conditions included varying field strengths, manufacturers, and reconstruction methods.

4.B.6. Multiparametric MRI (mpMRI) and imaging habitats

Cancer is a biologically complex and heterogeneous disease process.[186] As such, no single biomarker, imaging or otherwise, has yet to fully characterize or quantify this variation. mpMRI is a methodology that attempts to address this limitation by combining and processing individual MR biomarkers acquired within a given volume of interest. While still emerging as an oncologic methodology, mpMRI is expected to play a significant role in quantitative imaging, radiomics, machine learning, and decision support systems for such applications as tumor/organ segmentation for treatment planning, dose painting, tumor heterogeneity characterization/quantification, prognosis, outcome prediction, response assessment, and functionally adaptive RT.[207-212]

A novel application of mpMRI is the concept of imaging habitats within tumors and their surroundings. It comes from the application of landscape ecology principles to the evolutionary study of tumors, where cancer and normal cells under various selective forces (e.g., environmental conditions) form spatially distinct regions or habitats.[213] This approach attempts to relate macroscopic tissue heterogeneity from medical images to salient molecular properties of cells making up various ecosystems (i.e., habitats within a tumor and its surroundings).[214,215] Once defined based on the analysis of multiple different MRI sequences/parameters, these ecosystems can be spatially mapped back onto the images, providing a powerful 3D representation of the heterogeneity of a volume of interest that may be linked to biology to be further use in diagnosis and therapy.[216-218] Several groups have begun researching the link between MRI imaging habitats and histopathology and genomics, which could eventually lead to the use of imaging of volumetric "biopsies," thereby promising to revolutionize longitudinal histological characterization of tumors.[218-220]

An example of the creation and use of imaging habitats involves the combination of MR blood flow and cellular density biomarker information obtained from perfusion and fluid-attenuated inversion recovery (FLAIR) MRI. If the signal intensities in each scan are preprocessed and categorized as either high or low based on selected thresholds, four different habitats may be formed when each voxel is categorized.[221] The voxels denoting high cell density (low FLAIR) but poor perfusion may be interpreted as hypoxic regions or habitats for therapy resistant phenotypes, and if color coded, they are easily identifiable on axial images.[213,214]

Biomarker quantification: While mpMRI can provide quantitative outputs such as classifying regions of the brain as either being normal or abnormal as well as identifying CSF following stroke,[222] the significant variability of input MR biomarkers, processing techniques, and output parameters means that it currently does not qualify as a QIB. Further standardization and development, such as a QIBA profile, are therefore necessary to develop this promising methodology. Without this framework a biomarker Type cannot be assigned.

QA/QC: At the time of this report, standardized QA and QC methodologies and phantoms do not exist outside of those for individual biomarkers. As such, significant challenges exist with regard to reliably reproducing results among institutions that implement the "same" sequences, algorithms, and analyses. This challenge calls for the need to devote serious efforts in standardization of the complete process affecting the imaging biomarkers.[223-227]

mpMRI and habitats as biomarkers in radiation oncology: Cancer of the prostate is an active area of mpMRI research and clinical evaluation[228] The addition of ^{1}H MRSI to T_2-weighted MR imaging (AUC = 0.79) was shown to significantly improve the diagnostic accuracy of T_2-weighted MR imaging alone (AUC = 0.67) in the detection of locally recurrent prostate cancer after definitive external beam radiation therapy.[30] Figure 6 is an example of this combined approach reproduced from Zhang et al,[229] where the red arrows identify a region of decreased ADC in the right mid gland of the prostate. The T_2-weighted image shows no signal abnormality while the spectra overlapping the region of reduced ADC demonstrated an absence of citrate and polyamines and a very elevated Cho to Cr ratio.

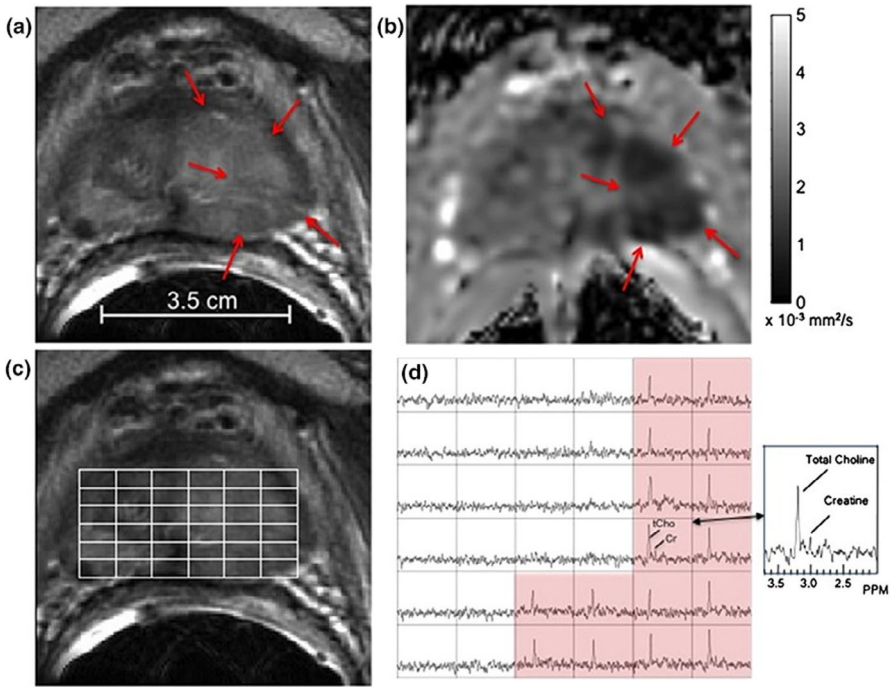

FIG. 6. (a) Representative T_2-weighted axial image of a 63-year-old patient with a PSA of 2.4 ng/ml, 2.5 years after external beam radiation therapy. (b) Corresponding ADC image. (c) T_2-weighted image with 0.16 cc ^{1}H MRSI spectral array overlaid. (d) Resultant ^{1}H spectra. The red arrows in image (b) indicate a region of clear-cut ADC reduction in the right mid gland of the prostate ($\leq 1.0 \times 10^{-3}$ mm^2/sec), which was not clear on the corresponding T_2-weighted image (A). Spectra overlapping the region of reduced ADC (c and d) demonstrated and absence of citrate and polyamines and a very elevated Cho to Cr ratio. A subsequent MR targeted trans urethral ultrasound-guided biopsy demonstrated a large volume of recurrent Gleason score 4 + 4 cancer in the same location as the ADC and metabolic abnormalities. Figure reproduced with permission from Zhang et al.[229] [Color figure can be viewed at wileyonlinelibrary.com]

mpMRI in general, and habitat imaging in particular, are expected to have many applications in RO. In radiotherapy, habitats have the potential to further enhance identification of gross tumor volume (GTV), clinical target volume (CTV), and planning target volume (PTV); and multiple habitats composing a tumor could each be treated to different doses (habitat-dose painting) based on the underlying imaging-derived biological information of each habitat. More importantly, imaging studies may be repeated at later times, revealing how habitats evolve due to therapy, affording the potential of identifying aggressive and/or resistant tumor regions dynamically, and therefore, the opportunity to adapt radiation doses based on the changing ecology of the tumor's habitats and its surrounding.[214,230,231]

Biomarker strengths, weaknesses, and limitations: A strength of mpMRI is the ability to combine multiple MR biomarkers and to process this information using advanced post processing techniques to improve the detection, differentiation, and therapeutic response of malignancies compared to a single MR biomarker. However, the weaknesses of mpMRI are associated with the qualitative nature of this approach as well as a lack of standardization in terms of biomarker selection, processing, and standardization. These, in combination with the fact that mpMRI is not yet considered a QIB, impose limitations on the applicability and translatability into clinical practice of mpMRI.

5. UNMET NEEDS AND RECOMMENDATIONS

Historically, diagnostic imaging systems lack the criteria necessary to be considered as quantitative measurement devices due to the absence of standardization protocols, requirements for quantifying a given characteristic, and methods to quantify the accuracy and precision of the characteristic (variable) under interrogation independent of measurement model and manufacturer. The establishment of imaging biomarkers has therefore provided a new impetus to transform this traditionally qualitative field into a quantitative one. This is particularly true regarding the development of quantitative MR biomarkers and their recent adaptation/integration into RO. Despite recent efforts (such as the QIBA initiative) in this arena, significant unmet or partially met needs necessary to complete this transformation remain. To help facilitate the transition, this task group has identified some of these needs and provided several recommendations intended to accelerate the development and integration of MR QIB into both clinical practice and RO research. These needs and related recommendations are of broad scope requiring long term and sustained efforts to address them. However, where appropriate short/intermediate term recommendations have been included to provide practical goals for advancing MR QIB development in RO. What follows are seven unmet or partially met needs identified, along with recommendations for the development and translation of MR biomarkers in RO.

Need #1:

QIBA profiles or equivalent for each biomarker pertinent to RO applications.

Recommendation #1:

Recognizing the need for further standardization and quantification of MR biomarkers, particularly their adaptation and adoption in RO, the committee recommends ongoing development of QIBA profiles including standardized QC/QA protocols and phantoms, focusing on the unique requirements of RO. QIBA Profiles, or equivalents, can and should be developed by organizations other than RSNA/QIBA. For example, the American Institute of Ultrasound in Medicine (AIUM) is collaborating with RSNA/QIBA to write Profiles for two ultrasound biomarkers. The European Biomarker Imaging Alliance (EIBALL) is collaborating with RSNA/QIBA to write a Profile for arterial spin label (ASL) MR imaging. QIBA-Japan is working on several QIBA-style Profiles. The methodology and recommendations for writing QIBA or QIBA-like Profiles are freely available on the web (https://qibawiki.rsna.org/index.php/Main_Page) and can be used or adapted by any interested entity.

Short/intermediate term: Provide recommendations on how to modify/adapt QIBA DWI profile to address specific needs of this QIB in RO. Encourage other relevant organizations, such as AAPM, ASTRO, and ISMRM, to create biomarker committees to write QIBA or QIBA-like Profiles.

Need #2:

Establish normative, disease, response to therapy, and toxicity values of valid MR QIB values when appropriate.

Recommendation #2:

As previously discussed, limited biomarker data satisfying QIBA protocols exists, particularly in regard to MR biomarker values of normative, disease, response to therapy, and normal tissue toxicity in RO, where applicable. Thus, the committee recommends ongoing efforts regarding integration of QIBA profiles into RO clinical trials so that values relevant to RO can be collected.

Short/intermediate term: Collect, tabulate, summarize and standardize reporting of DWI values (normative, disease, response to therapy, toxicity) for RO applications across multiple MR equipment manufacturers.

Need #3:

Standardized methods and reference materials to evaluate acquisition and analysis approaches used to determine QIB values.

Recommendation #3:

There remains significant variability in the phantoms, data acquisition methods, algorithms, and postprocessing applications used to provide MR QIB values. To address this limitation it is recommended that efforts be directed by professional societies including the AAPM, ISMRM, and RSNA to develop standardized algorithms and approaches to derive QIB values. In particular, a QIB must be able to produce values reproducible and independent of MR scanner manufacturer and postprocessing technique. Hence, end-to-end testing using standardized phantoms and acquisition methods should be performed in which the QIB value is known or predicted. In this way, variability as a function of field strength, MR scanner platform, and postprocessing algorithms can be tested without having access to proprietary information on the hardware and software used in acquisition and processing of the data.

Short/intermediate term: Evaluate QIBA MR phantoms (DWI, Relaxometry, elastography) for compatibility as applied to RO applications. Specifically in terms of quantitative values tested and the correlation with QIB values expected in RO applications. AAPM and ISMRM should continue, and ideally increase, their collaborative activities with the National Institute of Standards and Technology (NIST) to develop MR phantoms and to support the fledgling initiative of NIST to create a lending library of MR phantoms.

Need #4:

Additional educational materials and learning opportunities for both radiology and RO communities on the strengths, weaknesses, and challenges of the use of MR biomarkers in RO.

Recommendation #4:

Ongoing educational opportunities will be required to further advance the field of MR biomarkers in RO and ensure their appropriate and accurate use. To meet this need, the task group recommends multiple professional societies develop educational materials (such as web content, white papers, presentations at national, and international meetings) and educational opportunities (webinars, seminars, hands on learning). The task group also encourages the collaboration between various professional and government bodies associated with MR biomarker development through the sponsorship of joint educational seminars and academic/scientific meetings.

Short/intermediate term: Enhance MR in RO efforts currently underway in professional societies (AAPM, ISMRM) by promoting the inclusion of MR QIBs in educational activities.

Need #5:

Closer collaboration between clinical, academic, industry, and government agencies so as to expedite the development, testing and translation of MR biomarkers for RO clinical practice.

Recommendation #5:

A significant impediment to the translation of a biomarker from Type 0 to Type 2 (surrogate) is the cost of development including performing multicenter phase 3 clinical trials. The inability to implement appropriate clinical trials and the insufficient funding of them is a much greater threat to biomarker validation than are the limitations posed by the techniques to develop them. Therefore, the task group recommends that closer collaborations between professional societies (RSNA, AAPM, ISMRM, ASTRO) be established to help accelerate the development of MR biomarkers in RO and to identify and remove roadblocks that may impede biomarker development and progress. A tangible way to address this need would be to establish task forces/groups from all stakeholders, as well as the inclusion of MR biomarkers as a translational research

component of ongoing and future clinical trials. The committee also recommends encouraging closer collaboration between relevant government and nongovernmental health related agencies such as the Quantitative Imaging Network, Cancer Imaging Program, and Imaging and Radiation Oncology Core of the NIH and the American College of Radiology. In addition, closer collaboration amongst large cooperative clinical trial groups such as but not limited to the NRG (joint venture of the Radiation Therapy Oncology Group, the Gynecologic Oncology Group, and the National Surgical Breast and Bowel Project) and Children's Oncology Group is encouraged to evaluate, through clinical trials(phase 1, 2, and 3), promising biomarkers in RO.

Need #6:

Increased funding for biomarker development and clinical trials necessary to accelerate the transition of biomarkers from Type 0 to Type 2 (surrogate).

Recommendation #6:

Related to the previous need, the task group recognizes that additional funding will be needed to accelerate the development of promising MR imaging biomarkers in RO. This includes the funding of multicenter trials of MR biomarkers to establish the relationship between biomarker values and outcome. To meet this need, the task group recommends increased spending by government agencies at both state and federal levels, as well as by private foundations and professional organizations such as ASTRO, AAPM, and the RSNA.

Short/Intermediate term: At a minimum, all radiation therapy trials conducted by the NCI Cooperative Clinical Trials Network (NCCTN) should include at least a substudy to collect data relevant to one or more MR QIB's relevant to RO.

Need #7:

Standardization of MR biomarker data formats for importation and integration of biomarker information into RO treatment planning and decision-making systems.

Recommendation #7:

While the task group does not propose or provide guidance for the use of MR biomarkers currently as part of the clinical RO treatment planning and decision making process, it does realize that there exists the potential that such biomarkers, once classified as Type 2 to be used for this purpose at some future point in time. This will require the need to import biomarker information either as independent biomarker information or as some type of hybrid data into various RO systems. The task group therefore recommends the development of data format (e.g., DICOM RT) and import standards for this purpose by collaborative efforts between professional bodies and equipment manufacturers.

Short/intermediate term: Develop recommendations for importing DWI QIB data into RO systems so as to provide a template for future MR QIBs.

Need #8:

Development of a quantitative MR imaging system reconstruction pipeline.

Recommendation #8:

A constraint relating the development of QIBs is the fact that existing MR imaging systems are not designed as measurement systems but are rather engineered to provide high quality images in the smallest time interval possible. This has been a long-standing roadblock towards quantitative imaging and the clinical implementation of MR QIBs. The task group recommends that manufacturers in collaboration with the scientific community develop acquisition and reconstruction pipelines that are optimized to produce rigorous quantitative results thereby accelerating QIB development, testing, and clinical translation. This pipeline would be parallel to and independent of the standard reconstruction pipeline used for diagnostic imaging and interpretation.

6. CONCLUSIONS

MR biomarkers have the potential to improve the efficacy of radiation therapy treatments by means of improved diagnostic accuracy (i.e. detection of disease at an earlier stage), increased prognostic power (identifying imaging phenotypes that are correlated with improved outcome), and earlier detection of therapeutic response. This is particularly relevant to RO in which technological developments have enabled highly spatial and dose conformal treatments to be readily available and implementable. Under such conditions, QIBs of normal tissues at risk have the potential to provide the necessary information to ensure that such treatments do spare normal tissues and their function while ensuring the delivery of a sterilizing dose or radiation to malignant cells thereby increasing the therapeutic ratio. Conversely, the inappropriate or incorrect use of MR biomarker information can result in equally deleterious effects, resulting in the potential for misdiagnosis, incorrect treatment decisions, and negative treatment outcomes.

Correct application of biomarker information involves an understanding of the underlying biological processes that govern biomarker signals, the conditions under which a biomarker is quantifiable, the degree to which the biomarker has been validated, the extent the biomarker has been classified (as described in Table II), and the inherent limitation(s) of the QIB. While the temptation exists to simply use numeric information generated on the MR scanner or by the postprocessing of raw MR data straight "out of the box," this approach is fraught with danger, likely resulting in the negative treatment outcomes described above. It is most likely that the use of MR biomarkers in the radiation therapy decision process will be one in which they serve as one or more inputs into a multiparametric treatment decision process utilizing data from multiple sources, not just MR biomarker values.

7. SUMMARY

An MR biomarker is defined as any anatomic, physiologic, biochemical, or molecular parameter detectable with MR methods used to help establish the presence and/or severity of disease.[1] For an MR biomarker to be a QIB, it must produce a measurand considered to be either a ratio or interval variable.[6] This report provides an overview of existing and emergent RO MR biomarkers and their status both as a

QIB and their biomarker stage. Guidance is provided regarding MR biomarker use in RO. In this regard it should be apparent that few MR biomarkers can be considered as surrogates, meaning that the information provided by these biomarkers cannot be used as the single variable defining disease staging, type, extent, and response to therapy. Finally, the report provides direction regarding the establishment of the framework required to define and quantify biomarker values, most notably the formalization of this process as defined by QIBA and related biomarker profiles. Taken in full, these data indicate the potential, as well as pitfalls, associated with information obtained from MR data. A cautious approach is needed when using and integrating this data into the RO decision-making process.

ACKNOWLEDGMENTS

The authors wish to acknowledge the editorial assistance of Desiree J. Lanzino, PT, PhD.

CONFLICTS OF INTEREST

The members of TG294 listed below attest that they have no potential Conflicts of Interest related to the subject matter or materials presented in this document. Ken Hwang PhD, Daniel C. Sullivan M.D, John Kurhanewicz PhD, Yanle Hu PhD, Jihong Wang PhD, Wen Li PhD, Josef Debbins PhD, Eric Paulson PhD, Jeffrey R. Olsen M.D, Chia-ho Hua PhD, Lizette Warner Ph.D, Daniel Ma, MD, Eduardo Moros PhD, Neelam Tyagi PhD, Caroline Chung MD. Kiaran P. McGee PhD and the Mayo Clinic have intellectual property rights and a financial interest related to MR elastography technology.

[a]Author to whom correspondence should be addressed. Electronic mail: mcgee.kiaran@mayo.edu.

REFERENCES

1. Smith JJ, Sorensen AG, Thrall JH. Biomarkers in imaging: realizing radiology's future. *Radiology.* 2003;227:633–638.
2. Biomarkers Definitions Working Group. Biomarkers and surrogate endpoints: Preferred definitions and conceptual framework. *Clini Pharmacol Therapeut*. 2001;69:89–95.
3. Katz R. Biomarkers and surrogate markers: An FDA perspective. *NeuroRX*. 2004;1:189–195.
4. Frank R, Hargreaves R. Clinical biomarkers in drug discovery and development. *Nat Rev Drug Discov.* 2003;2:566–580.
5. Sorensen AG. Magnetic resonance as a cancer imaging biomarker. *J Clin Oncol*. 2006;24:3274–3281.
6. Sullivan DC, Obuchowski NA, Kessler LG, et al. Metrology standards for quantitative imaging biomarkers. *Radiology.* 2015;277:813–825.
7. Hunter DJ, Losina E, Guermazi A, Burstein D, Lassere MN, Kraus V. A pathway and approach to biomarker validation and qualification for osteoarthritis clinical trials. *Curr Drug Targets*. 2010;11:536–545.
8. O'Connor JPB, Aboagye EO, Adams JE, et al. Imaging biomarker roadmap for cancer studies. *Nat Rev Clin Oncol.* 2016;14:169. online publication.
9. McShane LM, Altman DG, Sauerbrei W, Taube SE, Gion M, Clark GM. REporting recommendations for tumour MARKer prognostic studies (REMARK). *Br J Cancer.* 2005;93:387–391.
10. Abramson RG, Burton KR, Yu J-P, et al. Methods and challenges in quantitative imaging biomarker development [published online ahead of print 2014/12/08]. *Acad Radiol*. 2015;22:25–32.
11. Mozley PD, Schwartz LH, Bendtsen C, Zhao B, Petrick N, Buckler AJ. Change in lung tumor volume as a biomarker of treatment response: a critical review of the evidence. *Annals of Oncology.* 2010;21:1751–1755.
12. Haveman LM, Ranft A, vd Berg H, et al. The relation of radiological tumor volume response to histological response and outcome in patients with localized Ewing Sarcoma. *Cancer Med*. 2019;8:1086–1094.
13. Therasse P, Arbuck SG, Eisenhauer EA, et al. New guidelines to evaluate the response to treatment in solid tumors. *JNCI: Journal of the National Cancer Institute*. 2000;92:205–216.
14. Eisenhauer EA, Therasse P, Bogaerts J, et al. New response evaluation criteria in solid tumours: revised RECIST guideline (version 1.1). *Eur J Cancer.* 2009;45:228–247.
15. Nishino M, Jagannathan JP, Ramaiya NH, Van den Abbeele AD. Revised RECIST guideline version 1.1: what oncologists want to know and what radiologists need to know. *Am J Roentgenol*. 2010;195 (2):281–289.
16. ACR. Phantom test guidance for use of the large MRI phantom for the American College of Radiology MRI accreditation program. Reston. VA; 2018.
17. Jackson EF, Bronskill MJ, Drost DJ, et al. Acceptance Testing and Quality Assurance Procedures for Magnetic Resonance Imaging Facilities, Report of MR Subcommittee Task Group I. College Park, MD: American Association of Physicists in Medicine; 2009.
18. Kleijn A, Chen JW, Buhrman JS, et al. Distinguishing inflammation from tumor and peritumoral edema by myeloperoxidase magnetic resonance imaging. *Clin Cancer Res.* 2011;17:4484–4493.
19. Bernstein MA, King KF, Zhou XJ. *Handbook of MRI Pulse Sequences*. Cambridge: Elsevier Academic Press; 2004.
20. Haacke EM, Brown RW, Thompson MR, Venkatesan R. *Magnetic Resonance Imaging: Physical Principals and Sequence Design*. New York, NY: John Wiley and Sons; 1999.
21. Does MD. Inferring brain tissue composition and microstructure via MR relaxometry. *NeuroImage*. 2018;182:136–148.
22. Barker PB, Bizzi A, De Stefano N, Gullapalli R, Lin DDM. *Clinical MR Spectroscopy: Techniques and Applications*. Cambridge, UK: Cambridge University Press; 2009.
23. Van Zijl PCM, Barker PB. Magnetic resonance spectroscopy and spectroscopic imaging for the study of brain metabolisma. *Ann N Y Acad Sci*. 1997;820:75–96.
24. Bottomley PA, Griffiths JR, eds. *Handbook of Magnetic Resonance Spectroscopy In Vivo: MRS Theory, Practice and Applications*. Chichester, UK: John Wiley & Sons Ltd; 2016.
25. Howe FA, Peet AC. Characterizing brain tumors by MRS. In: Bottomley PA, Griffiths JR, eds. *Handbook of Magnetic Resonance Spectroscopy In Vivo: MR Theory, Practice and Applications, Bottomley.* Chichester, UK: John Wiley & Sons Ltd; 2016:859–874.
26. Kurhanewicz J, Vigneron D. MRS in Prostate Cancer. In: Bottomley PA, Griffiths JR, eds. *Handbook of Magnetic Resonance Spectroscopy In Vivo: MR Theory, Practice and Applications, Bottomley.* Chichester, UK: John Wiley & Sons Ltd; 2016:997–1023.
27. Sharma U, Jagannathan NR. Breast Magnetic Resonance Spectroscopy (MRS). In: Bottomley PA, Griffiths JR, eds. *Handbook of Magnetic Resonance Spectroscopy In Vivo: MR Theory, Practice and Applications, Bottomley.* Chichester, UK: John Wiley & Sons Ltd; 2016:821–831.
28. Li Y, Lupo JM, Parvataneni R, et al. Survival analysis in patients with newly diagnosed glioblastoma using pre- and postradiotherapy MR spectroscopic imaging [published online ahead of print 2013/02/09]. *Neuro Oncol*. 2013;15:607–617.
29. Coakley FV, Teh HS, Qayyum A, et al. Endorectal MR imaging and MR spectroscopic imaging for locally recurrent prostate cancer after external beam radiation therapy: preliminary experience [published online ahead of print 2004/09/18]. *Radiology.* 2004;233:441–448.
30. Westphalen AC, Coakley FV, Roach M 3rd, McCulloch CE, Kurhanewicz J. Locally recurrent prostate cancer after external beam radiation therapy: diagnostic performance of 1.5-T endorectal MR imaging and MR spectroscopic imaging for detection [published online ahead of print 2010/06/17]. *Radiology.* 2010;256:485–492.

31. Di Costanzo A, Scarabino T, Trojsi F, et al. Multiparametric 3T MR approach to the assessment of cerebral gliomas: tumor extent and malignancy [published online ahead of print 2006/06/06]. *Neuroradiology.* 2006;48:622–631.
32. Salibi N, Brown MA. *Clinical MR Spectroscopy: First Principles*. New York, NY: Wiley-Liss; 1997.
33. Alger JR. Quantitative proton magnetic resonance spectroscopy and spectroscopic imaging of the brain: a didactic review. *Topics in magnetic resonance imaging : TMRI*. 2010;21:115–128.
34. McKnight TR, Noworolski SM, Vigneron DB, Nelson SJ. An automated technique for the quantitative assessment of 3D-MRSI data from patients with glioma. *J Magn Reson Imaging*. 2001;13:167–177.
35. Drost DJ, Riddle WR, Clarke GD. Proton magnetic resonance spectroscopy in the brain: report of AAPM MR Task Group #9 [published online ahead of print 2002/09/28]. *Med Phys*. 2002;29:2177–2197.
36. Hunjan S, Adalsteinsson E, Kim DH, et al. Quality assurance of magnetic resonance spectroscopic imaging–derived metabolic data. *Int J Radiat Oncol Biol Phys*. 2003;57:1159–1173.
37. Wilson M, Andronesi O, Barker PB, et al. Methodological consensus on clinical proton MRS of the brain: review and recommendations. *Magn Reson Med*. 2019;82:527–550.
38. Umbehr M, Bachmann LM, Held U, et al. Combined magnetic resonance imaging and magnetic resonance spectroscopy imaging in the diagnosis of prostate cancer: a systematic review and meta-analysis [published online ahead of print 2008/10/28]. *Eur Urol*. 2009;55:575–590.
39. Kurhanewicz J, Vigneron DB, Hricak H, Narayan P, Carroll P, Nelson SJ. Three-dimensional H-1 MR spectroscopic imaging of the in situ human prostate with high (0.24-0.7-cm3) spatial resolution [published online ahead of print 1996/03/01]. *Radiology.* 1996;198:795–805.
40. Kurhanewicz J, Swanson MG, Nelson SJ, Vigneron DB. Combined magnetic resonance imaging and spectroscopic imaging approach to molecular imaging of prostate cancer [published online ahead of print 2002/09/28]. *J Magn Reson Imaging*. 2002;16:451–463.
41. Westphalen AC, Coakley FV, Qayyum A, et al. Peripheral zone prostate cancer: accuracy of different interpretative approaches with MR and MR spectroscopic imaging [published online ahead of print 2007/11/21]. *Radiology.* 2008;246:177–184.
42. Zakian KL, Sircar K, Hricak H, et al. Correlation of proton MR spectroscopic imaging with gleason score based on step-section pathologic analysis after radical prostatectomy [published online ahead of print 2005/03/01]. *Radiology.* 2005;234:804–814.
43. Shukla-Dave A, Hricak H, Kattan MW, et al. The utility of magnetic resonance imaging and spectroscopy for predicting insignificant prostate cancer: an initial analysis [published online ahead of print 2007/01/17]. *BJU Int*. 2007;99:786–793.
44. Menard C, Susil RC, Choyke P, et al. MRI-guided HDR prostate brachytherapy in standard 1.5T scanner [published online ahead of print 2004/07/28]. *Int J Radiat Oncol Biol Phys*. 2004;59:1414–1423.
45. Pickles MD, Gibbs P, Lowry M, Turnbull LW. Diffusion changes precede size reduction in neoadjuvant treatment of breast cancer [published online ahead of print 2006/08/19]. *Magn Reson Imaging*. 2006;24:843–847.
46. Pouliot J, Kim Y, Lessard E, Hsu IC, Vigneron DB, Kurhanewicz J. Targeting dominant intraprostatic lesion using functional imaging with MR spectroscopy and high dose rate brachytherapy. *Radiother Oncol*. 2004;71:S120–S121.
47. Westphalen AC, McKenna DA, Kurhanewicz J, Coakley FV. Role of magnetic resonance imaging and magnetic resonance spectroscopic imaging before and after radiotherapy for prostate cancer [published online ahead of print 2008/03/28]. *J Endourol*. 2008;22:789–794.
48. McKenna DA, Coakley FV, Westphalen AC, et al. Prostate cancer: role of pretreatment MR in predicting outcome after external-beam radiation therapy–initial experience [published online ahead of print 2008/02/09]. *Radiology.* 2008;247:141–146.
49. Pickett B, Vigneault E, Kurhanewicz J, Verhey L, Roach M. Static field intensity modulation to treat a dominant intra-prostatic lesion to 90 Gy compared to seven field 3-dimensional radiotherapy [published online ahead of print 1999/07/01]. *Int J Radiat Oncol Biol Phys*. 1999;44:921–929.
50. van Lin EN, Futterer JJ, Heijmink SW, et al. IMRT boost dose planning on dominant intraprostatic lesions: gold marker-based three-dimensional fusion of CT with dynamic contrast-enhanced and 1H-spectroscopic MRI [published online ahead of print 2006/04/19]. *Int J Radiat Oncol Biol Phys*. 2006;65:291–303.
51. Xia P, Pickett B, Vigneault E, Verhey LJ, Roach M. Forward or inversely planned segmental multileaf collimator IMRT and sequential tomotherapy to treat multiple dominant intraprostatic lesions of prostate cancer to 90 Gy [published online ahead of print 2001/08/23]. *Int J Radiat Oncol Biol Phys*. 2001;51:244–254.
52. DiBiase SJ, Hosseinzadeh K, Gullapalli RP, et al. Magnetic resonance spectroscopic imaging-guided brachytherapy for localized prostate cancer [published online ahead of print 2002/03/02]. *Int J Radiat Oncol Biol Phys*. 2002;52:429–438.
53. Kim CK, Park BK, Han JJ, Kang TW, Lee HM. Diffusion-weighted imaging of the prostate at 3 T for differentiation of malignant and benign tissue in transition and peripheral zones: preliminary results [published online ahead of print 2007/06/01]. *J Comput Assist Tomogr.* 2007;31:449–454.
54. Pouliot J, Kim Y, Lessard E, Hsu IC, Vigneron DB, Kurhanewicz J. Inverse planning for HDR prostate brachytherapy used to boost dominant intraprostatic lesions defined by magnetic resonance spectroscopy imaging [published online ahead of print 2004/07/06]. *Int J Radiat Oncol Biol Phys*. 2004;59:1196–1207.
55. Zaider M, Zelefsky MJ, Lee EK, et al. Treatment planning for prostate implants using magnetic-resonance spectroscopy imaging [published online ahead of print 2000/06/23]. *Int J Radiat Oncol Biol Phys*. 2000;47:1085–1096.
56. Rabbani F, Stroumbakis N, Kava BR, Cookson MS, Fair WR. Incidence and clinical significance of false-negative sextant prostate biopsies [published online ahead of print 1998/03/21]. *J Urol*. 1998;159:1247–1250.
57. Cox JD, Kline RW. The lack of prognostic significance of biopsies after radiotherapy for prostatic cancer [published online ahead of print 1983/11/01]. *Semin Urol*. 1983;1:237–242.
58. Crook J, Malone S, Perry G, Bahadur Y, Robertson S, Abdolell M. Postradiotherapy prostate biopsies: what do they really mean? Results for 498 patients [published online ahead of print 2000/09/07]. *Int J Radiat Oncol Biol Phys*. 2000;48:355–367.
59. Kuban DA, El-Mardi AM, Schellhammer P. The significance of post-irradiation prostate biopsy with long-term follow-up [published online ahead of print 1992/01/01]. *Int J Radiat Oncol Biol Phys*. 1992;24:409–414.
60. Pickett B, Kurhanewicz J, Coakley F, Shinohara K, Fein B, Roach M, III. Use of MRI and spectroscopy in evaluation of external beam radiotherapy for prostate cancer [published online ahead of print 2004/11/03]. *Int J Radiat Oncol Biol Phys*. 2004;60:1047–1055.
61. Roach M, Kurhanewicz J, Carroll P. Spectroscopy in prostate cancer: hope or hype? [published online ahead of print 2002/01/05]. *Oncology (Williston Park)*. 2001;15:1399–1410; discussion 1415-1396, 1418.
62. Westphalen AC, Reed GD, Vinh PP, Sotto C, Vigneron DB, Kurhanewicz J. Multiparametric 3T endorectal mri after external beam radiation therapy for prostate cancer [published online ahead of print 2012/04/27]. *J Magn Reson Imaging*. 2012;36:430–437.
63. McKnight TR, von dem Bussche MH, Vigneron DB, et al. Histopathological validation of a three-dimensional magnetic resonance spectroscopy index as a predictor of tumor presence [published online ahead of print 2002/10/31]. *J Neurosurg*. 2002;97:794–802.
64. Chang SM, Nelson S, Vandenberg S, et al. Integration of preoperative anatomic and metabolic physiologic imaging of newly diagnosed glioma [published online ahead of print 2009/04/10]. *J Neurooncol*. 2009;92:401–415.
65. Anwar M, Molinaro AM, Morin O, et al. Identifying voxels at risk for progression in glioblastoma based on dosimetry, physiologic and metabolic MRI [published online ahead of print 2017/07/21]. *Radiat Res*. 2017;188:303–313.
66. Chuang CF, Chan AA, Larson D, et al. Potential value of MR spectroscopic imaging for the radiosurgical management of patients with recurrent high-grade gliomas [published online ahead of print 2007/09/20]. *Technol Cancer Res Treat*. 2007;6:375–382.
67. Pirzkall A, McKnight TR, Graves EE, et al. MR-spectroscopy guided target delineation for high-grade gliomas [published online ahead of print 2001/06/29]. *Int J Radiat Oncol Biol Phys*. 2001;50:915–928.

68. Chan AA, Lau A, Pirzkall A, et al. Proton magnetic resonance spectroscopy imaging in the evaluation of patients undergoing gamma knife surgery for Grade IV glioma [published online ahead of print 2004/09/09]. *J Neurosurg*. 2004;101:467–475.
69. Einstein DB, Wessels B, Bangert B, et al. Phase II trial of radiosurgery to magnetic resonance spectroscopy-defined high-risk tumor volumes in patients with glioblastoma multiforme [published online ahead of print 2012/03/27]. *Int J Radiat Oncol Biol Phys*. 2012;84:668–674.
70. Chawla S, Wang S, Kim S, et al. Radiation injury to the normal brain measured by 3D-echo-planar spectroscopic imaging and diffusion tensor imaging: initial experience [published online ahead of print 2013/11/28]. *J Neuroimaging*. 2015;25:97–104.
71. Jeon JY, Kovanlikaya I, Boockvar JA, et al. Metabolic response of glioblastoma to superselective intra-arterial cerebral infusion of bevacizumab: a proton MR spectroscopic imaging study [published online ahead of print 2012/05/12]. *AJNR Am J Neuroradiol*. 2012;33:2095–2102.
72. Quon H, Brunet B, Alexander A, et al. Changes in serial magnetic resonance spectroscopy predict outcome in high-grade glioma during and after postoperative radiotherapy [published online ahead of print 2011/10/04]. *Anticancer Res*. 2011;31:3559–3565.
73. Tarnawski R, Sokol M, Pieniazek P, et al. 1H-MRS in vivo predicts the early treatment outcome of postoperative radiotherapy for malignant gliomas [published online ahead of print 2002/04/17]. *Int J Radiat Oncol Biol Phys*. 2002;52:1271–1276.
74. Harris LM, Davies NP, MacPherson L, et al. Magnetic resonance spectroscopy in the assessment of pilocytic astrocytomas [published online ahead of print 2008/10/07]. *Eur J Cancer*. 2008;44:2640–2647.
75. Steffen-Smith EA, Shih JH, Hipp SJ, Bent R, Warren KE. Proton magnetic resonance spectroscopy predicts survival in children with diffuse intrinsic pontine glioma [published online ahead of print 2011/05/14]. *J Neurooncol*. 2011;105:365–373.
76. Elias AE, Carlos RC, Smith EA, et al. MR spectroscopy using normalized and non-normalized metabolite ratios for differentiating recurrent brain tumor from radiation injury [published online ahead of print 2011/08/09]. *Acad Radiol*. 2011;18:1101–1108.
77. Fink JR, Carr RB, Matsusue E, et al. Comparison of 3 Tesla proton MR spectroscopy, MR perfusion and MR diffusion for distinguishing glioma recurrence from posttreatment effects [published online ahead of print 2011/10/18]. *J Magn Reson Imaging*. 2012;35:56–63.
78. Aribal E, Asadov R, Ramazan A, Ugurlu MU, Kaya H. Multiparametric breast MRI with 3T: Effectivity of combination of contrast enhanced MRI, DWI and 1H single voxel spectroscopy in differentiation of Breast tumors. *Eur J Radiol*. 2016;85:979–986.
79. Huang J, Wang A-M, Shetty A, et al. Differentiation between intra-axial metastatic tumor progression and radiation injury following fractionated radiation therapy or stereotactic radiosurgery using MR spectroscopy, perfusion MR imaging or volume progression modeling. *Magn Reson Imaging*. 2011;29:993–1001.
80. Isobe T, Matsumura A, Anno I, et al. Quantification of cerebral metabolites in glioma patients with proton MR spectroscopy using T2 relaxation time correction. *Magn Reson Imaging*. 2002;20:343–349.
81. Ken S, Vieillevigne L, Franceries X, et al. Integration method of 3D MR spectroscopy into treatment planning system for glioblastoma IMRT dose painting with integrated simultaneous boost [published online ahead of print 2013/01/03]. *Radiat Oncol*. 2013;8.
82. Kurhanewicz J, Vigneron DB, Nelson SJ, et al. Citrate as an in vivo marker to discriminate prostate cancer from benign prostatic hyperplasia and normal prostate peripheral zone: detection via localized proton spectroscopy [published online ahead of print 1995/03/01]. *Urology*. 1995;45:459–466.
83. Pirzkall A, Nelson SJ, McKnight TR, et al. Metabolic imaging of low-grade gliomas with three-dimensional magnetic resonance spectroscopy [published online ahead of print 2002/07/20]. *Int J Radiat Oncol Biol Phys*. 2002;53:1254–1264.
84. Wilson M, Cummins CL, MacPherson L, et al. Magnetic resonance spectroscopy metabolite profiles predict survival in paediatric brain tumours. *Eur J Cancer*. 2013;49:457–464.
85. Bossuyt PM, Reitsma JB, Bruns DE, et al. The STARD statement for reporting studies of diagnostic accuracy: explanation and elaboration [published online ahead of print 2003/01/07]. *Ann Intern Med*. 2003;138:W1–12.
86. Lin AP, Tran TT, Ross BD. Impact of evidence-based medicine on magnetic resonance spectroscopy [published online ahead of print 2006/06/10]. *NMR Biomed*. 2006;19:476–483.
87. Hagmann P, Jonasson L, Maeder P, Thiran J-P, Wedeen VJ, Meuli R. Understanding diffusion mr imaging techniques: from scalar diffusion-weighted imaging to diffusion tensor imaging and beyond. *Radiographics*. 2006;26:S205–S223.
88. Westin CF, Maier SE, Mamata H, Nabavi A, Jolesz FA, Kikinis R. Processing and visualization for diffusion tensor MRI [published online ahead of print 2002/06/05]. *Med Image Anal*. 2002;6:93–108.
89. Alexander AL, Lee JE, Lazar M, Field AS. Diffusion tensor imaging of the brain. *Neurotherapeutics*. 2007;4:316–329.
90. Jerome NP, Papoutsaki M-V, Orton MR, et al. Development of a temperature-controlled phantom for magnetic resonance quality assurance of diffusion, dynamic, and relaxometry measurements. *Med Phys*. 2016;43:2998–3007.
91. Liu B, Zhu T, Zhong J. Comparison of quality control software tools for diffusion tensor imaging [published online ahead of print 2014/12/03]. *Magn Reson Imaging*. 2015;33:276–285.
92. Baliyan V, Das CJ, Sharma RU, Gupta AK. Diffusion weighted imaging: Technique and applications. *World J Radiol*. 2016;8:785–798.
93. Schnapauff D, Zeile M, Niederhagen MB, et al. Diffusion-weighted echo-planar magnetic resonance imaging for the assessment of tumor cellularity in patients with soft-tissue sarcomas. *J Magn Reson Imaging*. 2009;29:1355–1359.
94. White NS, McDonald CR, Farid N, et al. Diffusion-weighted imaging in cancer: Physical foundations and applications of Restriction Spectrum Imaging. *Can Res*. 2014;74:4638–4652.
95. Elson A, Bovi J, Siker M, Schultz C, Paulson E. Evaluation of absolute and normalized apparent diffusion coefficient (ADC) values within the post-operative T2/FLAIR volume as adverse prognostic indicators in glioblastoma [published online ahead of print 2015/02/24]. *J Neurooncol*. 2015;122:549–558.
96. Ito J, Marmarou A, Barzo P, Fatouros P, Corwin F. Characterization of edema by diffusion-weighted imaging in experimental traumatic brain injury [published online ahead of print 1996/01/01]. *J Neurosurg*. 1996;84:97–103.
97. Barzo P, Marmarou A, Fatouros P, Hayasaki K, Corwin F. Contribution of vasogenic and cellular edema to traumatic brain swelling measured by diffusion-weighted imaging [published online ahead of print 1997/12/31]. *J Neurosurg*. 1997;87:900–907.
98. Han H, Han C, Wu X, et al. Preoperative grading of supratentorial nonenhancing gliomas by high b-value diffusion-weighted 3 T magnetic resonance imaging [published online ahead of print 2017/04/26]. *J Neurooncol*. 2017;133:147–154.
99. Pujol S, Wells W, Pierpaoli C, et al. The DTI challenge: toward standardized evaluation of diffusion tensor imaging tractography for neurosurgery. *J Neuroimaging*. 2015;25:875–882.
100. Miles KA. Tumour angiogenesis and its relation to contrast enhancement on computed tomography: a review [published online ahead of print 1999/08/19]. *Eur J Radiol*. 1999;30:198–205.
101. Belliveau JW, Rosen BR, Kantor HL, et al. Functional cerebral imaging by susceptibility-contrast NMR [published online ahead of print 1990/06/01]. *Magn Reson Med*. 1990;14:538–546.
102. Rosen BR, Belliveau JW, Vevea JM, Brady TJ. Perfusion imaging with NMR contrast agents [published online ahead of print 1990/05/01]. *Magn Reson Med*. 1990;14:249–265.
103. Boxerman JL, Hamberg LM, Rosen BR, Weisskoff RM. MR contrast due to intravascular magnetic susceptibility perturbations [published online ahead of print 1995/10/01]. *Magn Reson Med*. 1995;34:555–566.
104. Detre JA, Leigh JS, Williams DS, Koretsky AP. Perfusion imaging [published online ahead of print 1992/01/01]. *Magn Reson Med*. 1992;23:37–45.
105. Kwong KK, Chesler DA, Weisskoff RM, et al. Mr perfusion studies with t1-weighted echo planar imaging. *Magn Reson Med*. 1995;34:878–887.
106. Morse OC, Singer JR. Blood velocity measurements in intact subjects [published online ahead of print 1970/10/23]. *Science*. 1970;170:440–441.
107. Williams DS, Detre JA, Leigh JS, Koretsky AP. Magnetic resonance imaging of perfusion using spin inversion of arterial water [published

online ahead of print 1992/01/01]. *Proc Natl Acad Sci USA*. 1992;89:212–216.
108. Boxerman JL, Schmainda KM, Weisskoff RM. Relative cerebral blood volume maps corrected for contrast agent extravasation significantly correlate with glioma tumor grade, whereas uncorrected maps Do Not. *Am J Neuroradiol*. 2006;27:859–867.
109. Donahue KM, Krouwer HGJ, Rand SD, et al. Utility of simultaneously acquired gradient-echo and spin-echo cerebral blood volume and morphology maps in brain tumor patients [published online ahead of print 2000/06/22]. *Magn Reson Med*. 2000;43:845–853.
110. Law M, Yang S, Babb JS, et al. Comparison of cerebral blood volume and vascular permeability from dynamic susceptibility contrast-enhanced perfusion MR imaging with glioma grade [published online ahead of print 2004/05/14]. *AJNR Am J Neuroradiol*. 2004;25:746–755.
111. Schmainda KM, Rand SD, Joseph AM, et al. Characterization of a first-pass gradient-echo spin-echo method to predict brain tumor grade and angiogenesis. *Am J Neuroradiol*. 2004;25:1524–1532.
112. Jahng GH, Li KL, Ostergaard L, Calamante F. Perfusion magnetic resonance imaging: a comprehensive update on principles and techniques. *Korean J Radiol*. 2014;15:554–577.
113. Jackson EF, Gupta SN, Rosen MA, et al. QIBA DCE-MRI technical committee update: phantom studies and first DCE-MRI profile. Paper presented at: Radiological Society of North America2010; Chicago, Ill.
114. Matsuo M, Matsumoto S, Mitchell JB, Krishna MC, Camphausen K. Magnetic resonance imaging of the tumor microenvironment in radiotherapy: perfusion, hypoxia, and metabolism. *Semin Radiat Oncol*. 2014;24:210–217.
115. Cuenod CA, Fournier L, Balvay D, Guinebretiere JM. Tumor angiogenesis: pathophysiology and implications for contrast-enhanced MRI and CT assessment. *Abdom Imaging*. 2006;31:188–193.
116. Chen HY, Larson PEZ, Bok RA, et al. Assessing Prostate Cancer Aggressiveness with Hyperpolarized Dual-Agent 3D Dynamic Imaging of Metabolism and Perfusion [published online ahead of print 2017/04/22]. *Cancer Res*. 2017;77:3207–3216.
117. Reske SN, Blumstein NM, Neumaier B, et al. Imaging prostate cancer with 11C-choline PET/CT. *J Nucl Med*. 2006;47:1249–1254.
118. Futterer JJ, Heijmink SW, Scheenen TW, et al. Prostate cancer localization with dynamic contrast-enhanced MR imaging and proton MR spectroscopic imaging. *Radiology*. 2006;241:449–458.
119. Kozlowski P, Chang SD, Jones EC, Berean KW, Chen H, Goldenberg SL. Combined diffusion-weighted and dynamic contrast-enhanced MRI for prostate cancer diagnosis–correlation with biopsy and histopathology. *J Magn Reson Imaging*. 2006;24:108–113.
120. Huang W, Li X, Chen Y, et al. Variations of dynamic contrast-enhanced magnetic resonance imaging in evaluation of breast cancer therapy response: a multicenter data analysis challenge. *Transl Oncol*. 2014;7:153–166.
121. Walker-Samuel S, Leach MO, Collins DJ. Evaluation of response to treatment using DCE-MRI: the relationship between initial area under the gadolinium curve (IAUGC) and quantitative pharmacokinetic analysis. *Phys Med Biol*. 2006;51:3593–3602.
122. Quantitative Imaging Biomarker Alliance. Profile: DCE MRI quantification. http://qibawiki.rsna.org/images/7/7b/DCEMRIProfile_v1_6-20111213.pdf
123. Kleppesto M, Larsson C, Groote I, et al. T2*-correction in dynamic contrast-enhanced MRI from double-echo acquisitions. *J Magn Reson Imaging*. 2014;39:1314–1319.
124. Mouridsen K, Emblem KE, Bjørnerud A, Jennings D, Sorensen AG. Subject-specific AIF optimizes reproducibility of perfusion parameters in longitudinal DSC-MRI in comparison to session and population level AIF. In. International Society of Magnetic Resonance in Medicine; 2011.
125. Planey CR, Welch EB, Xu L, et al. Temporal sampling requirements for reference region modeling of DCE-MRI data in human breast cancer. *J Magn Reson Imaging*. 2009;30:121–134.
126. Cao Y. The promise of dynamic contrast-enhanced imaging in radiation therapy. *Semin Radiat Oncol*. 2011;21:147–156.
127. Ogawa S, Lee TM, Kay AR, Tank DW. Brain magnetic resonance imaging with contrast dependent on blood oxygenation. *Proc Natl Acad Sci*. 1990;87:9868–9872.
128. Thulborn KR, Waterton JC, Matthews PM, Radda GK. Oxygenation dependence of the transverse relaxation time of water protons in whole blood at high field. *Biochimica et Biophysica Acta (BBA) - General Subjects*. 1982;714:265–270.
129. Gabriel M, Brennan NP, Peck KK, Holodny AI. Blood oxygen level dependent functional magnetic resonance imaging for presurgical planning. *Neuroimaging Clin N Am*. 2014;24:557–571.
130. Medina LS, Bernal B, Dunoyer C, et al. Seizure disorders: functional MR imaging for diagnostic evaluation and surgical treatment–prospective study [published online ahead of print 2005/07/01]. *Radiology*. 2005;236:247–253.
131. Friston KJ, Holmes AP, Worsley KJ, Poline JP, Frith CD, Frackowiak RSJ. Statistical parametric maps in functional imaging: A general linear approach. *Hum Brain Mapp*. 1994;2:189–210.
132. Biswal B, Zerrin Yetkin F, Haughton VM, Hyde JS. Functional connectivity in the motor cortex of resting human brain using echo-planar mri. *Magn Reson Med*. 1995;34(4):537–541.
133. Friedman L, Glover GH. Report on a multicenter fMRI quality assurance protocol [published online ahead of print 2006/05/02]. *J Magn Reson Imaging*. 2006;23:827–839.
134. Liu TT, Glover GH, Mueller BA, et al. Quality assurance in functional MRI. In: Uludag K. Ugurbil K. eds. *fMRI: From Nuclear Spins to Brain Functions. Biological Magnetic Resonance*. Vol 30. Boston, MA: Springer; 2015.
135. Glover GH, Mueller BA, Turner JA, et al. Function biomedical informatics research network recommendations for prospective multicenter functional MRI studies [published online ahead of print 2012/02/09]. *J Magn Reson Imaging*. 2012;36:39–54.
136. Greve DN, Mueller BA, Liu T, et al. A novel method for quantifying scanner instability in fMRI [published online ahead of print 2011/03/18]. *Magn Reson Med*. 2011;65:1053–1061.
137. Hallac RR, Zhou H, Pidikiti R, et al. Correlations of noninvasive BOLD and TOLD MRI with pO2 and relevance to tumor radiation response [published online ahead of print 2013/07/03]. *Magn Reson Med*. 2014;71:1863–1873.
138. O'Connor JPB, Robinson SP, Waterton JC. Imaging tumour hypoxia with oxygen-enhanced MRI and BOLD MRI [published online ahead of print 2019/01/24]. *Br J Radiol*. 2019;92:20180642.
139. Wang M, Ma H, Wang X, et al. Integration of BOLD-fMRI and DTI into radiation treatment planning for high-grade gliomas located near the primary motor cortexes and corticospinal tracts. *Radiat Oncol*. 2015;10:64.
140. Rieke V, Butts PK. MR thermometry. *J Magn Reson Imaging*. 2008;27:376–390.
141. Quesson B, de Zwart JA, Moonen CTW. Magnetic resonance temperature imaging for guidance of thermotherapy. *J Magn Reson Imaging*. 2000;12:525–533.
142. Gorny KR, Hangiandreou NJ, Hesley GK, Gostout BS, McGee KP, Felmlee JP. MR guided focused ultrasound: technical acceptance measures for a clinical system [published online ahead of print 2006/06/08]. *Phys Med Biol*. 2006;51:3155–3173.
143. Farahani K, Stafford J, Chopra R. AAPM task group 241 – MR-guided focused ultrasound. *Journal of Therapeutic Ultrasound*. 2015;3:O70.
144. Kim Y. Advances in MR image-guided high-intensity focused ultrasound therapy. *Int J Hyperth*. 2015;31:225–232.
145. ter Haar G. Safety first: progress in calibrating high-intensity focused ultrasound treatments. *Imaging in Medicine*. 2013;5:567–575.
146. Liu G, Song X, Chan KW, McMahon MT. Nuts and bolts of chemical exchange saturation transfer MRI [published online ahead of print 2013/01/11]. *NMR Biomed*. 2013;26:810–828.
147. Jones KM, Pollard AC, Pagel MD. Clinical applications of chemical exchange saturation transfer (CEST) MRI. *J Magn Reson Imaging*. 2018;47:11–27.
148. Wu B, Warnock G, Zaiss M, et al. An overview of CEST MRI for non-MR physicists. *EJNMMI Physics*. 2016;3:19.
149. Chen M, Chen C, Shen Z, et al. Extracellular pH is a biomarker enabling detection of breast cancer and liver cancer using CEST MRI [published online ahead of print 2017/05/16]. *Oncotarget*. 2017;8:45759–45767.
150. Harris RJ, Cloughesy TF, Liau LM, et al. Simulation, phantom validation, and clinical evaluation of fast pH-weighted molecular imaging using amine chemical exchange saturation transfer echo planar imaging (CEST-EPI) in glioma at 3 T [published online ahead of print 2016/10/19]. *NMR Biomed*. 2016;29:1563–1576.

151. Chan KW, Jiang L, Cheng M, et al. CEST-MRI detects metabolite levels altered by breast cancer cell aggressiveness and chemotherapy response [published online ahead of print 2016/04/22]. *NMR Biomed*. 2016;29:806–816.
152. Yao J, Tan CHP, Schlossman J, et al. pH-weighted amine chemical exchange saturation transfer echoplanar imaging (CEST-EPI) as a potential early biomarker for bevacizumab failure in recurrent glioblastoma [published online ahead of print 2019/02/27]. *J Neurooncol*. 2019;142:587–595.
153. Miloushev VZ, Keshari KR, Holodny AI. Hyperpolarization MRI: preclinical models and potential applications in neuroradiology. *Topics Magn Res Imaging*. 2016;25:31–37.
154. Kurhanewicz J, Vigneron DB, Brindle K, et al. Analysis of cancer metabolism by imaging hyperpolarized nuclei: prospects for translation to clinical research. *Neoplasia*. 2011;13:81–97.
155. Sriram R, Kurhanewicz J, Vigneron DB. Hyperpolarized 13C MRI and MRS studies. In: Bottomley PA, Griffiths JR, eds. *Handbook of Magnetic Resonance Spectroscopy In Vivo: MRS Theory, Practice and Applications*. Chichester, UK: John Wiley & Sons Ltd; 2016:659–678.
156. Aggarwal R, Vigneron DB, Kurhanewicz J. Hyperpolarized 1-[(13)C]-Pyruvate magnetic resonance imaging detects an early metabolic response to androgen ablation therapy in prostate cancer. *Eur Urol*. 2017;72:1028–1029.
157. Nelson SJ, Kurhanewicz J, Vigneron DB, et al. Metabolic imaging of patients with prostate cancer using hyperpolarized [1-13C]Pyruvate. *Sci Transl Med*. 2013;5:198ra108.
158. Daniels CJ, McLean MA, Schulte RF, et al. A comparison of quantitative methods for clinical imaging with hyperpolarized (13)C-pyruvate. *NMR Biomed*. 2016;29:387–399.
159. Izquierdo-Garcia JL, Viswanath P, Eriksson P, et al. IDH1 mutation induces reprogramming of pyruvate metabolism. *Cancer Res*. 2015;75:2999–3009.
160. Wilson DM, Keshari KR, Larson PEZ, et al. Multi-compound polarization by DNP allows simultaneous assessment of multiple enzymatic activities in vivo. *J Magn Reson*. 2010;205:141–147.
161. Chen L, Ye Y, Chen H, et al. Dynamic contrast-enhanced magnetic resonance imaging for differentiating between primary tumor, metastatic node and normal tissue in head and neck cancer. *Curr Med Imaging Rev*. 2018;14:416–421.
162. Albers MJ, Bok R, Chen AP, et al. Hyperpolarized 13C lactate, pyruvate, and alanine: noninvasive biomarkers for prostate cancer detection and grading. *Cancer Res*. 2008;68:8607–8615.
163. Witney TH, Kettunen MI, Brindle KM. Kinetic modeling of hyperpolarized 13C label exchange between pyruvate and lactate in tumor cells [published online ahead of print 2011/05/21]. *J Biolog Chem*. 2011;286:24572–24580.
164. Mariotti E, Veronese M, Dunn JT, Southworth R, Eykyn TR. Kinetic analysis of hyperpolarized data with minimum a priori knowledge: Hybrid maximum entropy and nonlinear least squares method (MEM/NLS) [published online ahead of print 2014/07/22]. *Magn Reson Med*. 2015;73:2332–2342.
165. Harris T, Eliyahu G, Frydman L, Degani H. Kinetics of hyperpolarized 13C1-pyruvate transport and metabolism in living human breast cancer cells [published online ahead of print 2009/10/15]. *Proc Natl Acad Sci U S A*. 2009;106:18131–18136.
166. Harrison C, Yang C, Jindal A, et al. Comparison of kinetic models for analysis of pyruvate-to-lactate exchange by hyperpolarized 13 C NMR [published online ahead of print 2012/03/28]. *NMR Biomed*. 2012;25:1286–1294.
167. Hill DK, Orton MR, Mariotti E, et al. Model free approach to kinetic analysis of real-time hyperpolarized 13C magnetic resonance spectroscopy data. *PLoS One*. 2013;8:e71996.
168. Khegai O, Schulte RF, Janich MA, et al. Apparent rate constant mapping using hyperpolarized [1-(13)C]pyruvate [published online ahead of print 2014/08/27]. *NMR Biomed*. 2014;27:1256–1265.
169. Walker CM, Lee J, Ramirez MS, Schellingerhout D, Millward S, Bankson JA. A catalyzing phantom for reproducible dynamic conversion of hyperpolarized [1-(1)(3)C]-pyruvate [published online ahead of print 2013/08/27]. *PLoS One*. 2013;8:e71274.
170. Kurhanewicz J, Vigneron DB, Ardenkjaer-Larsen JH, et al. Hyperpolarized (13)C MRI: path to clinical translation in oncology [published online ahead of print 2018/11/23]. *Neoplasia*. 2019;21:1–16.
171. Walker CM, Merritt M, Wang J-X, Bankson JA. Use of a multicompartment dynamic single enzyme phantom for studies of hyperpolarized magnetic resonance agents. *JoVE*. 2016:e53607.
172. Day SE, Kettunen MI, Cherukuri MK, et al. Detecting response of rat C6 glioma tumors to radiotherapy using hyperpolarized [1- 13C]pyruvate and 13C magnetic resonance spectroscopic imaging [published online ahead of print 2011/01/26]. *Magn Reson Med*. 2011;65:557–563.
173. Chen AP, Chu W, Gu Y-P, Cunnhingham CH. Probing early tumor response to radiation therapy using hyperpolarized [1-(13)C]pyruvate in MDA-MB-231 Xenografts. *PLoS One*. 2013;8:e56551.
174. Sandulache VC, Chen Y, Lee J, et al. Evaluation of hyperpolarized [1-13C]-pyruvate by magnetic resonance to detect ionizing radiation effects in real time. *PLoS One*. 2014;9:e87031.
175. Sandulache VC, Skinner HD, Wang Y, et al. Glycolytic inhibition alters anaplastic thyroid carcinoma tumor metabolism and improves response to conventional chemotherapy and radiation. *Mol Cancer Ther*. 2012;11:1373–1380.
176. Cunningham CH, Lau JY, Chen AP, et al. Hyperpolarized 13C metabolic MRI of the human heart: initial experience. *Circ Res*. 2016;119:1177–1182.
177. Miloushev VZ, Granlund KL, Boltyanskiy R, et al. Metabolic imaging of the human brain with hyperpolarized 13C pyruvate demonstrates 13C lactate production in brain tumor patients [published online ahead of print 2018/05/18]. *Cancer Res*. 2018;78:3755–3760.
178. Park I, Larson PEZ, Gordon JW, et al. Development of methods and feasibility of using hyperpolarized carbon-13 imaging data for evaluating brain metabolism in patient studies. *Magn Reson Med*. 2018;80:864–873.
179. Moghbel MC, Kostakoglu L, Zukotynski K, et al. Response assessment criteria and their applications in lymphoma: part 1 [published online ahead of print 2016/04/30]. *J Nucl Med*. 2016;57:928–935.
180. Muthupillai R, Lomas DJ, Rossman PJ, Greenleaf JF, Manduca A, Ehman RL. Magnetic resonance elastography by direct visualization of propagating acoustic strain waves. *Science*. 1995;269:1854–1857.
181. Manduca A, Oliphant TE, Dresner MA, et al. Magnetic resonance elastography: non-invasive mapping of tissue elasticity [published online ahead of print 2001/12/04]. *Med Image Anal*. 2001;5:237–254.
182. Cox TR, Erler JT. Remodeling and homeostasis of the extracellular matrix: implications for fibrotic diseases and cancer. *Disease Models Mech*. 2011;4:165–178.
183. Shieh AC. Biomechanical forces shape the tumor microenvironment. *Ann Biomed Eng*. 2011;39:1379–1389.
184. Yu H, Mouw JK, Weaver VM. Forcing form and function: biomechanical regulation of tumor evolution. *Trends Cell Biol*. 2011;21:47–56.
185. Huang X, Yang N, Fiore VF, et al. Matrix stiffness-induced myofibroblast differentiation is mediated by intrinsic mechanotransduction. *Am J Respir Cell Mol Biol*. 2012;47:340–348.
186. Weinberg RA. *The Biology of Cancer*, 2nd edn. New York, New York: Garland Science; 2013.
187. Fung YC. *Biomechanics: Mechanical Properties of Living Tissues*. New York: Springer-Verlag; 1993.
188. Oliphant TE, Manduca A, Ehman RL, Greenleaf JF. Complex-valued stiffness reconstruction for magnetic resonance elastography by algebraic inversion of the differential equation. *Magn Reson Med*. 2001;45:299–310.
189. Low G, Kruse SA, Lomas DJ. General review of magnetic resonance elastography. *World J Radiol*. 2016;8:59–72.
190. Pepin KM, Chen J, Glaser KJ. et al. MR elastography derived shear stiffness-a new imaging biomarker for the assessment of early tumor response to chemotherapy. *Magn Res Med*. 2014;71:1834–1840.
191. Pepin KM, Ehman RL, McGee KP. Magnetic resonance elastography (MRE) in cancer: technique, analysis, and applications. *Prog Nucl Magn Reson Spectrosc*. 2015;91:32–48.
192. Reiss-Zimmermann M, Streitberger K-J, Sack I, et al. High resolution imaging of viscoelastic properties of intracranial tumours by multifrequency magnetic resonance elastography. *Clin Neuroradiol*. 2015;25:371–378.

193. Pepin KM, Arani A, Fattahi N, et al. Noninvasive Characterization and Staging of Glioma with MR Elastography - A Pilot Study. Paper presented at: Internation Society of Magnetic Resonance in Medicine Annual Meeting; Toronto, CA; 2015.
194. Cassidy FH, Yokoo T, Aganovic L, et al. Fatty liver disease: mr imaging techniques for the detection and quantification of liver steatosis. *Radiographics*. 2009;29:231–260.
195. Hamilton G, Middleton MS, Bydder M, et al. Effect of PRESS and STEAM sequences on magnetic resonance spectroscopic liver fat quantification. *J Magn Reson Imaging*. 2009;30:145–152.
196. Yoo YH, Kim HS, Lee YH, et al. Comparison of multi-echo dixon methods with volume interpolated breath-hold gradient echo magnetic resonance imaging in fat-signal fraction quantification of paravertebral muscle [published online ahead of print 2015/08/21]. *Korean J Radiol*. 2015;16:1086–1095.
197. Yu H, McKenzie CA, Shimakawa A, et al. Multiecho reconstruction for simultaneous water-fat decomposition and T2* estimation. *J Magn Reson Imaging*. 2007;26:1153–1161.
198. Reeder SB, Hu HH, Sirlin CB. Proton density fat-fraction: a standardized MR-based biomarker of tissue fat concentration [published online ahead of print 2012/07/11]. *J Magn Reson Imaging*. 2012;36:1011–1014.
199. Kühn J-P, Hernando D, Meffert PJ, et al. Proton-density fat fraction and simultaneous R2* estimation as an MRI tool for assessment of osteoporosis. *Eur Radiol*. 2013;23:3432–3439.
200. McCullough AJ. Update on nonalcoholic fatty liver disease [published online ahead of print 2002/03/02]. *J Clin Gastroenterol*. 2002;34:255–262.
201. van Gemert WA, Monninkhof EM, May AM, et al. Association between changes in fat distribution and biomarkers for breast cancer. *Endocr Relat Cancer*. 2017;24:297–305.
202. White DL, Kanwal F, El–Serag HB. Association between nonalcoholic fatty liver disease and risk for hepatocellular cancer, based on systematic Review. *Clin Gastroenterol Hepatol*. 2012;10:1342–1359.
203. Bolan PJ, Arentsen L, Sueblinvong T, et al. Water-fat mr imaging for assessing changes in bone marrow composition due to radiation and chemotherapy in gynecologic cancer patients. *J Magn Reson Imaging*. 2013;38.
204. Carmona R, Pritz J, Bydder M, et al. Fat composition changes in bone marrow during chemotherapy and radiotherapy. *Int J Radiat Oncol Biol Phys*. 2014;90:155–163.
205. Guiu B, Petit JM, Bonnetain F, et al. Visceral fat area is an independent predictive biomarker of outcome after first-line bevacizumab-based treatment in metastatic colorectal cancer [published online ahead of print 2009/10/20]. *Gut*. 2010;59:341–347.
206. Ladoire S, Bonnetain F, Gauthier M, et al. Visceral fat area as a new independent predictive factor of survival in patients with metastatic renal cell carcinoma treated with antiangiogenic agents [published online ahead of print 2011/01/08]. *Oncologist*. 2011;16:71–81.
207. Jaffray DA, Das S, Jacobs PM, Jeraj R, Lambin P. How advances in imaging will affect precision radiation oncology. *Int J Radiat Oncol Biol Phys*. 2018;101:292–298.
208. van der Heide UA, Houweling AC, Groenendaal G, Beets-Tan RG, Lambin P. Functional MRI for radiotherapy dose painting. *Magn Reson Imaging*. 2012;30:1216–1223.
209. Owrangi AM, Greer PB, Glide-Hurst CK. MRI-only treatment planning: benefits and challenges. *Phys Med Biol*. 2018;63:05TR01.
210. Viswanath S, Tiwari P, Chappelow J, Toth R, Kurhanewicz J, Madabhushi A. CADOnc((c)): an integrated toolkit for evaluating radiation therapy related changes in the prostate using multiparametric MRI. *Proc IEEE Int Symp Biomed Imaging*. 2011;2011:2095–2098.
211. Mason J, Al-Qaisieh B, Bownes P, et al. Multi-parametric MRI-guided focal tumor boost using HDR prostate brachytherapy: a feasibility study. *Brachytherapy*. 2014;13:137–145.
212. Zhou H, Zhang Z, Denney R, et al. Tumor physiological changes during hypofractionated stereotactic body radiation therapy assessed using multi-parametric magnetic resonance imaging. *Oncotarget*. 2017;8:37464–37477.
213. Kim JY, Gatenby RA. Quantitative clinical imaging methods for monitoring intratumoral evolution. *Methods Mol Biol*. 2017;1513:61–81.
214. Gatenby RA, Grove O, Gillies RJ. Quantitative imaging in cancer evolution and ecology. *Radiology*. 2013;269:8–15.
215. Maley CC, Aktipis A, Graham TA, et al. Classifying the evolutionary and ecological features of neoplasms. *Nat Rev Cancer*. 2017;17:605–619.
216. Chang Y-C, Ackerstaff E, Tschudi Y, et al. Delineation of tumor habitats based on dynamic contrast enhanced MRI. *Sci Rep*. 2017;7:9746.
217. Sala E, Mema E, Himoto Y, et al. Unravelling tumour heterogeneity using next-generation imaging: radiomics, radiogenomics, and habitat imaging. *Clin Radiol*. 2017;72:3–10.
218. Chaudhury B, Zhou MU, Goldgof DB, et al. Heterogeneity in intratumoral regions with rapid gadolinium washout correlates with estrogen receptor status and nodal metastasis. *J Magn Reson Imaging*. 2015;42:1421–1430.
219. Stoyanova R, Pollack A, Takhar M, et al. Association of multiparametric MRI quantitative imaging features with prostate cancer gene expression in MRI-targeted prostate biopsies. *Oncotarget*. 2016;7:53362–53376.
220. Lee J, Narang S, Martinez J, Rao G, Rao A. Spatial habitat features derived from multiparametric magnetic resonance imaging data are associated with molecular subtype and 12-month survival status in glioblastoma multiforme. *PLoS One*. 2015;10:e0136557.
221. Zhou M, Chaudhury B, Hall LO, Goldgof DB, Gillies RJ, Gatenby RA. Identifying spatial imaging biomarkers of glioblastoma multiforme for survival group prediction. *J Magn Reson Imaging*. 2017;46:115–123.
222. Jacobs MA, Mitsias P, Soltanian-Zadeh H, et al. Multiparametric MRI tissue characterization in clinical stroke with correlation to clinical outcome. *Part 2*. 2001;32:950–957.
223. Newitt DC, Malyarenko D, Chenevert TL, et al. Multisite concordance of apparent diffusion coefficient measurements across the NCI Quantitative Imaging Network. *J Med Imaging (Bellingham)*. 2018;5:011003.
224. Deng J, Wang Y. Quantitative magnetic resonance imaging biomarkers in oncological clinical trials: Current techniques and standardization challenges. *Chronic Dis Transl Med*. 2017;3:8–20.
225. Joint H. Neck radiotherapy MRIDC. a multi-institutional comparison of dynamic contrast-enhanced magnetic resonance imaging parameter calculations. *Sci Rep*. 2017;7:11185.
226. Obuchowski NA, Reeves AP, Huang EP, et al. Quantitative imaging biomarkers: a review of statistical methods for computer algorithm comparisons. *Stat Methods Med Res*. 2015;24:68–106.
227. Raunig DL, McShane LM, Pennello G, et al. Quantitative imaging biomarkers: a review of statistical methods for technical performance assessment. *Stat Methods Med Res*. 2015;24:27–67.
228. Hegde JV, Mulkern RV, Panych LP, et al. Multiparametric MRI of prostate cancer: An update on state-of-the-art techniques and their performance in detecting and localizing prostate cancer. *J Magn Reson Imaging*. 2013;37:1035–1054.
229. Zhang VY, Westphalen A, Delos Santos L, et al. The role of metabolic imaging in radiation therapy of prostate cancer [published online ahead of print 2013/08/14]. *NMR Biomed*. 2014;27:100–111.
230. Dextraze K, Saha A, Kim D, et al. Spatial habitats from multiparametric MR imaging are associated with signaling pathway activities and survival in glioblastoma. *Oncotarget*. 2017;8:112992–113001.
231. You D, Kim MM, Aryal MP, et al. Tumor image signatures and habitats: a processing pipeline of multimodality metabolic and physiological images. *J Med Imaging (Bellingham)*. 2018;5:011009.

SUPPORTING INFORMATION

Additional Supporting Information may be found online in the Supporting Information section at the end of the article.

Appendix A1. MR biomarker adaptation example: Apparent Diffusion Coefficient

Appendix A2. Contrast agents and mechanisms

Appendix A3. Survey of MR biomarkers in radiation oncology